CHARACTERIZATION OF MECHANICAL PROPERTIES OF COPPER COVETIC WIRES

BY

GABRIELA JEANNETTE COUVERTIER SANTOS

THESIS

Submitted in partial fulfillment of the requirements
for the degree of Master of Science in Mechanical Engineering
in the Graduate College of the
University of Illinois at Urbana-Champaign, 2017

Urbana, Illinois

Adviser:

Professor Iwona M. Jasiuk

ABSTRACT

Copper and copper alloys are commonly used in various applications because of their ability to be formed and their excellent thermal and electrical properties. A new copper carbon alloy, called copper covetic, is showing promising properties. Copper covetic materials were prepared Third Millennium Metals, Inc., by adding carbon to molten copper 10200 while a DC current was applied. The samples had 3, 5, and 9 weight percent of carbon, as reported by manufacturers. We refer to them as CuC3, CuC5, and CuC9, respectively. Copper 10200 wire with no added carbon created using normal wire making processes was used as comparison and is referred to as CuC0.

The samples were tested using a nanoindenter at a 10,000uN and 5,000uN maximum load. The nanoindentation test showed a decrease of elastic modulus as the maximum applied load increased. The highest value of elastic modulus for both loads was for the CuC5 sample, and the lowest value was for the CuC9 sample. The microindentation test performed at a 500 Pond load resulted in the CuC3 sample having the highest hardness and the CuC0 and CuC5 samples having the lowest hardness.

The tensile test results showed an increase yield stress and ultimate tensile strength for the CuC3, CuC5, and CuC9 samples. The CuC3 and CuC9 samples had higher yield stress and ultimate tensile strength than the CuC5 and CuC0 sample. The elastic modulus values of all samples were low in comparison to other copper alloys. The fracture strain for the CuC5, CuC3, and CuC9 samples were lower than the CuC0 sample. A CuC9 thin sample was prepared in a Dual-Beam Focus Ion Beam for analysis in a Transmission Electron Microscope (TEM). The diffraction and images generated by the TEM show the possibility of carbon being incorporated into the copper sample. The results show promise for covetics for various industrial applications.

ACKNOWLEDGEMENTS

I would like to thank my advisor Dr. Iwona M. Jasiuk, whose guidance these past years help make this project and thesis possible.

This research was carried out in part in the Frederick Seitz Materials Research Laboratory (MRL) Central Research Facilities, University of Illinois. I would particularly like to thank two staff members of the MRL, Kathleen A. Walsh and Dr. Elvan Ekiz-Stumphy, for their constant assistance and prompt help in answering all my questions.

Lastly but not least, I would like to thank my Father and parents for their constant support.

TABLE OF CONTENTS

CHAPTER 1: COPPER AND COPPER ALLOYS

1.1 Copper Overview

Copper is a widely used metal due to its superior thermal and electrical properties. Also, it has an excellent ability to be molded and cast. Because of these attributes, copper is used in 50% of the United States production of electrical wiring [1]. The general process of extracting copper from copper ores has many steps for refinement and purifying. Copper sulfides are heated to matte, copper and iron sulfates, using reverberatory furnaces. This matte is then formed into blisters by adding air to the process. The copper is then refined by heat resulting in a tough pitch copper. The pitch copper is then electrolytically refined. This last step changes 30% copper to a 99.95% copper [1].

Alloyed copper can have a considerable increase in strength, but also a decrease in ductility and conductivity. Brasses are formed by combining copper and zinc. As the weight percent of zinc increases so does the strength and resistance to corrosion. This happens up to a certain weight percent after which these properties will reduce with the further addition of zinc. Other properties, such as electrical conductivity, will consistently decrease with the addition of zinc [2]. Bronzes are formed by alloying tin and copper, aluminum and copper, and silicon and copper. Bronzes have increased strength and corrosion resistance but are more costly than brasses. Copper-nickel alloys also improve yield strength, endurance limit, and tensile strength. Beryllium-copper can have an increased strength which can increase even more after precipitation hardening [1].

Copper alloys strength values are presented in Table 1.1 [1] [3]. The yield strength of pure copper ranges from 69MPa to 365 MPa, while copper alloys yield strength varies from 76

MPa to 1048 MPa. The ultimate tensile strength of pure copper ranges from 228 MPa to 455 MPa and yield strength of different copper alloys varies from 248 MPa to 1400 MPa. The copper alloy with the highest ultimate tensile strength is a nickel-copper in both wrought and cast forms. The copper alloy with the highest yield strength is a wrought high copper alloy. The elastic modulus of copper and some copper alloys are presented in Table 1.2. Beryllium-copper has the highest elastic modulus with a 159 GPa value. Free cutting brass has the lowest value of elastic modulus with 96 GPa.

Table 1.1 General properties of copper and copper alloys.

Alloy	UNS No.	Nominal composition	Treatment	Ultimate tensile strength		Yield strength		Elongation, %	Rockwell hardness
				MPa	ksi	MPa	Ksi		
Pure copper									
Oxygen-free high conductivity	C10200	99.95 Cu	...	228–455	33–66	69–365	10–53	55–4	...
High-copper alloys									
Beryllium-copper	C17200	97.9Cu-1.9Be-0.2Ni or Co	Annealed	490	71	...	...	35	60 HRB
			Hardened	1400	203	1048	152	2	42 HRC
Brass									
Gilding, 95%	C21000	95Cu-5Zn	Annealed	248	36	76	11	45	52 HRF
			Hard	393	57	352	51	5	64 HRB
Red brass, 85%	C23000	85Cu-15Zn	Annealed	283	41	90	13	47	64 HRF
			Hard	434	63	407	59	5	73 HRB
Cartridge brass, 70%	C26000	70Cu-30Zn	Annealed	359	52	131	19	55	72 HRF
			Hard	531	77	441	64	8	82 HRB
Muntz metal	C28000	60Cu-40Zn	Annealed	379	55	117	17	45	80 HRF
			Half-hard	490	71	352	51	15	75 HRB
High-lead brass	C35300	62Cu-36Zn-2Pb	Annealed	352	51	117	17	52	68 HRF
			Hard	421	61	317	46	7	80 HRB
Bronze									
Phosphor bronze, 5%	C51000	95Cu-5Sn	Annealed	352	51	172	25	55	40 HRB
			Hard	586	85	579	84	9	90 HRB
Phosphor bronze, 10%	C52400	90Cu-10Sn	Annealed	483	70	248	36	63	62 HRB
			Hard	710	103	655	95	16	96 HRB
Aluminum bronze	C60800	95Cu-5Al	Annealed	421	61	172	25	66	49 HRB
			Cold rolled	703	102	441	64	8	94 HRB
Aluminum bronze	C63000	81.5Cu-9.5Al-5Ni-2.5Fe-1Mn	Extruded	689	100	414	60	15	96 HRB
			Half-hard	814	118	517	75	15	98 HRB
High-silicon bronze	C65500	96Cu-3Si-1Mn	Annealed	441	64	214	31	55	66 HRB
			Hard	655	95	407	59	8	95 HRB
Copper-nickel									
Cupronickel, 30%	C71500	70Cu-30Ni	Annealed	386	56	124	18	36	40 HRB
			Cold rolled	586	85	552	80	3	86 HRB
Nickel silver									
Nickel silver	C75700	65Cu-23Zn-12Ni	Annealed	427	62	193	28	35	55 HRB
			Hard	593	86	524	76	4	89 HRB

Taken from Elements of metallurgy and engineering alloys [1].

The process of cold working, plastic deformation of metals while at cold temperature (non-melting temperature), causes an increase in yield and tensile strengths. Cold working can increase the yield strength of copper and its alloys up to six times [1]. Annealing of a copper or

a copper alloy after cold working can help bring the material to a more malleable form. These processes are used to further improve a specific pure copper or a specific alloy.

Table 1.2 Range of tensile elastic modulus of copper and copper alloys.

Metal	Form	Elastic Modulus (GPa)
copper oxygen free	strip	117
tough pitch copper	strip	117
beryllium copper	strip	159
cadmium copper	wire	124
aluminum brass	tube, plate	110
brasses (CuZn)	strip	102-115
free cutting brass	rod	96
nickel silvers	strip	121-124
phosphor bronzes	strip, wire	111-122
aluminum bronzes	plate, rod, strip	111-131
copper-nickels	tube, plate	132-152
silicon bronzes	plate, rod	103

Taken from Smithells metals reference book [11].

1.2 Copper and Carbon

With the constant need to improve old and new technology, the pursuit of better alloys has risen. Although many copper alloys exist, the increased demand and price of this metal have sprouted great interest to create better copper alloys. Recent studies have tried to combine copper with carbon. The goal of creating such an alloy is to strengthen the metal while trying to maintain copper's ductility and conductivity.

Some research has focused on creating a metal-carbon powder to make composites by deposition methods. Guiderdoni et al. [4] used spark plasma sintering of copper with double-walled carbon nanotubes to create a copper-carbon composite. Guiderdoni reported finding

agglomerate of carbon and dendritical copper in the composite. In that research, the samples with added carbon had an increased friction coefficient in aluminum and steel ball test and double the Vickers microhardness when compared to pure copper samples. Ullbrand et al. [5] found that the uniformity of the carbon-copper mixture was slightly less dependent on the method, spark plasma sintering or hot pressing, but more directly related to the quality of coating and type of carbon. In Ullbrand's research platelet structure carbon nanofibres generated large agglomerates but few in number. In contrast, herringbone structure carbon nanofibres had a larger number of smaller sized agglomerates. Ullbrand also found that independently of the carbon used, the thermal conductivity decreased as the amount of carbon increased.

Copper-carbon composites may have application limitations because of temperature. Increasing temperature can cause carbon to separate from the copper, causing the material properties to go back to those of the original copper. Covetics, studied in this thesis, are metal-carbon alloys which are created in a different way and the carbon is retained even when heated. Covetics are formed by adding carbon into a molten metal while some form of electrical energy is being applied. This material is said to form a single phase that does not separate with elevated temperature [6]. Salamanca Riba et al [7] investigated silver covetics to find if the carbon and silver formed a chemical reaction when a current is applied to the molten metal, known as electromitigation. Different tests, such as Raman spectroscopy and x-ray photoelectron spectroscopy, showed that the carbon formed different lattice structures and seemed to incorporate well with the silver. Also importantly, the silver covetic retained its weight when heated after a slight initial weight lost, showing that the carbon stays incorporated even after heating. In another investigation performed by Isaacs et al. [8], copper covetics were used to create thin films. The films were created using e-beam deposition over silicon substrates. These

films showed better conductivity and less oxidation when compared to pure copper thin film samples.

1.3 Preparation of Copper Covetic Wire

To create the covetic samples a specific weight percent of carbon was added to oxygen-free Copper 10200, 99.5% pure copper. The copper carbon metals were then remelted while a 300 amps DC current was applied. Next, the molten metal was poured into a 0.20 m diameter chilled mold. The 0.20 m diameter billet surfaces were cleaned. After cleaning the samples were extruded in a Bayway extruder at 871 ^{o}C to 0.01 m diameter rods. The rods were then water quenched to room temperature. After the rods cooled to room temperature, the samples were processed through a two-die drawing machine at room temperature and aged using a GE bell annealer at 537 ^{o}C for two hours. This drawing and aging process was repeated two more times, each time reducing the diameter of the rods. The produced wire samples measured diameters are provided later (Chapter 2). Copper wires with 3, 5, and 9 weight percent of carbon added during manufacturing were prepared, and will be referred to as CuC3, CuC5, CuC9, respectively. For comparison, a normal Cu 10200 wire of similar diameter manufactured using conventional methods and no added carbon was used. This sample will be referred to as CuC0.

CHAPTER 2: TENSILE TEST

2.1 Introduction

The tensile test is a common test performed to measure mechanical properties of materials. Tensile test records the force being applied as a function of displacement. The stress at a given point in time is found using Equation 2.1

$$\sigma_i = P_i / A_o \tag{2.1}$$

where P_i is the load at a time i and A_o is the original cross-sectional area. Most materials have a recoverable elastic region and an unrecoverable plastic region. The yield point is where there is a materials transition from the elastic region to the plastic region. The yield stress for metal is most commonly found using the 0.2% offset technique as illustrated in Figure 2.1. The ultimate tensile stress, σ_{UTS}, which is the maximum stress the material can withhold, can be calculated using Equation 2.2

$$\sigma_{UTS} = P_{max} / A_o \tag{2.2}$$

where P_{max} is the maximum applied load. The strain is a measurement used to describe the change in displacement. Engineering strain is defined as

$$\varepsilon = \Delta l / l_o \tag{2.3}$$

where Δl is the change in length and l_o is the original length. The elastic modulus, E, is found from the slope of an elastic portion of the stress-strain curve as described by Equation 2.4

$$E = \Delta\sigma_{elastic} / \Delta\varepsilon_{elastic} \tag{2.4}$$

where $\Delta\varepsilon_{elastic}$ is the strain difference in the elastic region and $\Delta\sigma_{elastic}$ is the stress difference in the elastic region [22]. The yield stress, UTS, and elastic modulus can be seen on an engineering stress versus engineering strain graph in Figure 2.1.

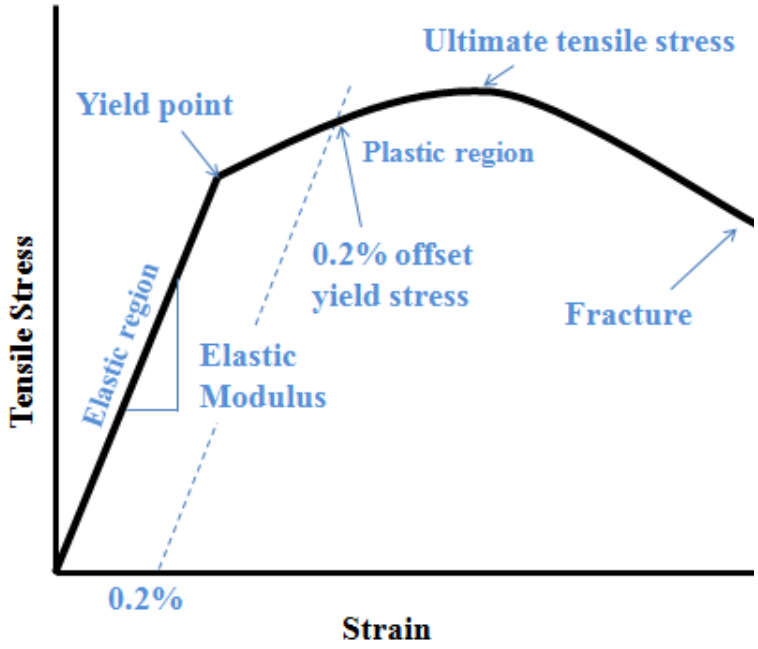

Figure 2.1 Representative engineering stress and engineering strain graph for metals.

2.2 Method

Four samples of each weight percent of carbon were tested using a Servo Hydraulic Material Testing Machine (MTS Systems Corporation, Eden Prairie, Minnesota). The setup for the tensile test can be seen in Figure 2.2. A 0.5 m long wire was wrapped around stable wheels on the top and bottom of the test fixture. For additional stability, four small plastic plates clamped fixture on the top and bottom of the strain gauge, without touching the gauge. The load was applied at a strain rate of 0.0015"/min. Tensile load was applied to the sample wires until they broke. The average and standard deviation of the results values were then calculated. After the tensile test was performed, the samples' fracture surfaces were viewed using a scanning electron microscope (SEM) model JEOL 6060 (JEOL, Akishima, Tokyo, Japan).

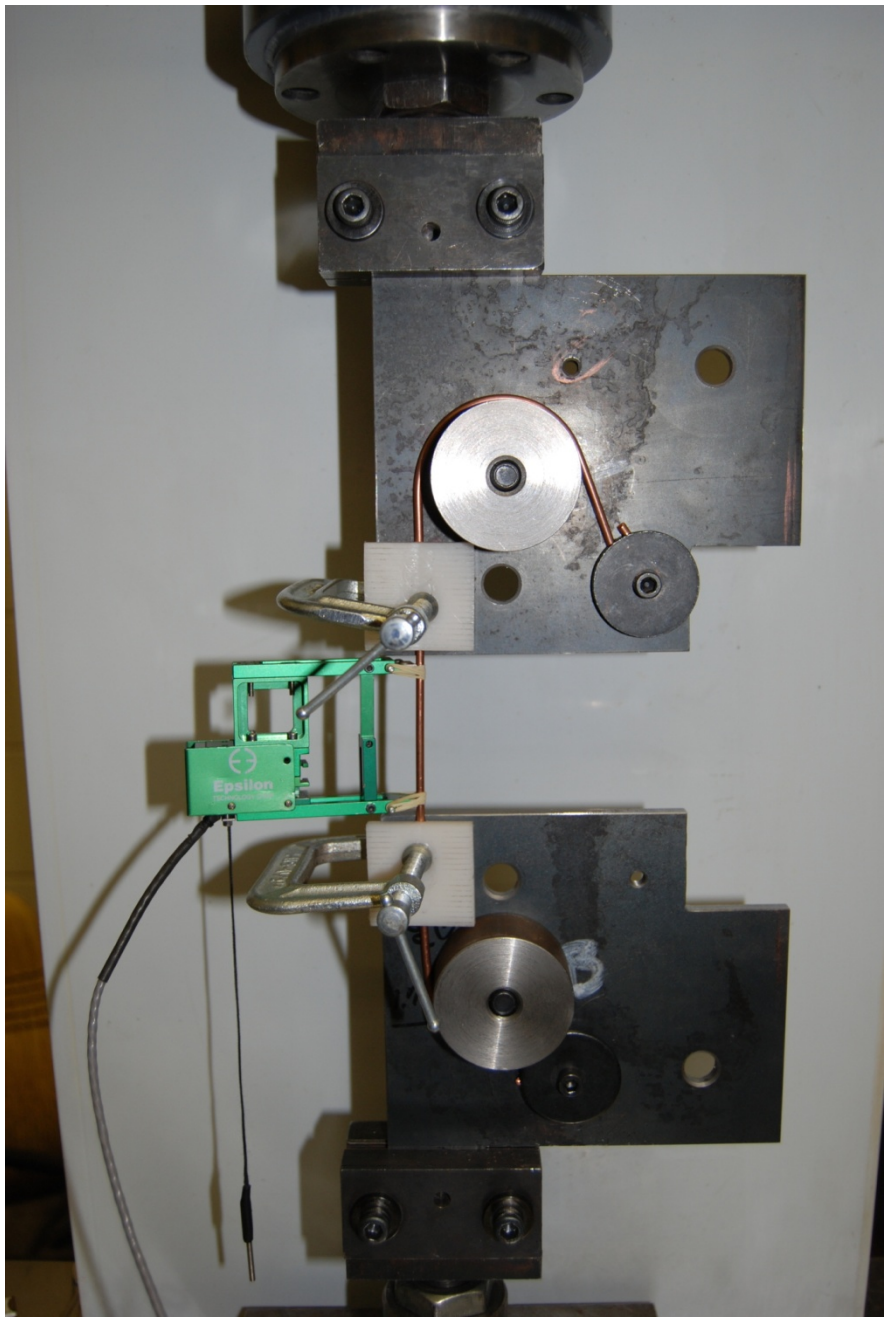

Figure 2.2. Copper wire tensile test sample setup.

2.3 Results and Discussion

The diameter and test section length of the wire samples were measured before the tensile test. The original area of the circular cross section was then calculated from the diameter measurement, Table 2.1. The individual area of each sample was used for stress calculations.

Table 2.1 Copper wire dimensions before testing.

Sample	Sample Number	Diameter (mm)	Area of Specimen (mm^2)	Original Length (mm)
CuC0	sample 1	3.07	7.42	133.8
	sample 2	3.1	7.55	134.8
	sample 3	3.07	7.42	134.8
	sample 4	3.07	7.42	133.9
CuC3	sample 1	3.12	7.68	134.7
	sample 2	3.12	7.68	133.0
	sample 3	3.12	7.68	134.6
	sample 4	3.12	7.68	135.1
CuC5	sample 1	3.15	7.81	134.3
	sample 2	3.15	7.81	132.9
	sample 3	3.15	7.81	134.0
	sample 4	3.15	7.81	134.4
CuC9	sample 1	3.15	7.81	134.2
	sample 2	3.18	7.94	133.9
	sample 3	3.15	7.81	134.0
	sample 4	3.18	7.94	133.7

Using the data generated by the tensile test, the ultimate strength, elastic modulus, and 0.2% yield stress were calculated. The tensile test results are presented in Table 2.2, Table 2.3 and Figure 2.3 using the average and standard deviation. The average yield stresses were 122 MPa, 217 MPa, 201 MPa, 210 MPa for CuC0, CuC3, CuC5, and CuC9, respectively. The average ultimate tensile stresses of the samples were 276 MPa, 418 MPa, 405 MPa, 423 MPa for CuC0, CuC3, CuC5, and CuC9, respectively. The results for the copper covetics show an increase in yield stress and ultimate tensile stress for CuC3, CuC5, and CuC9 compared to the CuC0. The CuC3 samples had the highest yield stress, while the CuC9 samples had the highest ultimate tensile stress.

Table 2.2 Load and stress tensile test results for copper wires.

Sample	Value	Max Load (N)	UTS (MPa)	Yield Stress (GPa)	Elastic Modulus (GPa)
Cu0C	average	2059.5	276.6	122.1	32.4
	std dev	8.8	2.8	14.8	2.3
Cu3C	average	3207.1	418.5	217.9	35.0
	std dev	13.3	2.1	7.3	1.2
Cu5C	average	3158.2	405.9	201.8	32.5
	std dev	8.8	1.5	15.5	0.9
Cu9C	average	3322.8	423.5	210.0	34.7
	std dev	8.8	4.4	9.9	0.8

When compared to copper alloys presented in Table 1.2, the values of yield stresses for the CuC3, CuC5, and CuC9 covetics are similar to annealed high silicon bronze and higher than most annealed brasses. The ultimate tensile stresses of the covetic samples are higher than most annealed brass and very similar to most hard brasses.

The elastic modulus was slightly greater in CuC3, CuC5, and CuC9 compared to the CuC0. In Table 1.1, the copper alloys presented have elastic modulus between 96 to 159 GPa. The results from the current tensile test of copper wires in Table 2.2 show a maximum elastic modulus of 35 GPa for the CuC5 sample. This includes the CuC0 sample which only obtained an elastic modulus value of 32 GPa. The samples seem to be more elastic than ordinary copper. It is worth noting that the values presented in Table 1.2 are for different dimensions and shapes of copper alloy samples.

Table 2.3 Displacement and strain tensile test results for copper wires.

Sample	Value	Elongation of Specimen (mm)	Strain at Fracture
Cu0C	average	23.31	0.173
	std dev	0.73	0.005
Cu3C	average	1.37	0.01
	std dev	0.05	0.0004
Cu5C	average	1.54	0.011
	std dev	0.22	0.001
Cu9C	average	1.52	0.011
	std dev	0.17	0.001

The elongation of the samples, the difference between the final length and the original length, were 23.31 mm, 1.37 mm, 1.54 mm, 1.52 mm for CuC0, CuC3, CuC5, and CuC9 samples respectively, as seen in Table 2.3. The strain at the moment of fracture was 0.17 m/m, 0.01 m/m, 0.01 m/m, 0.01 m/m for CuC0, CuC3, CuC5, and CuC9 samples, respectively. The elongation and strain at moment of fracture for the CuC3, CuC5, and CuC9 samples were lower than the CuC0 sample.

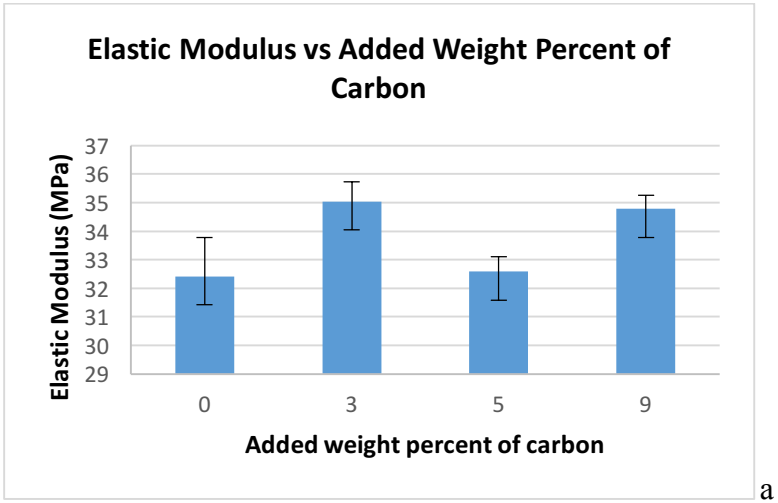

a

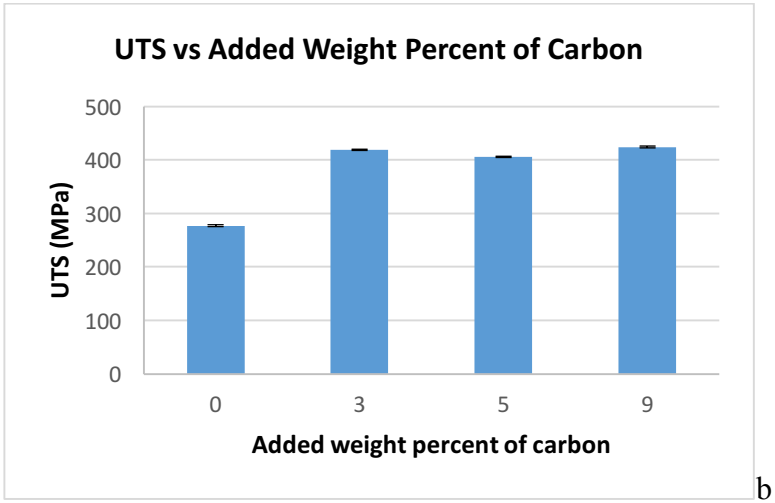

b

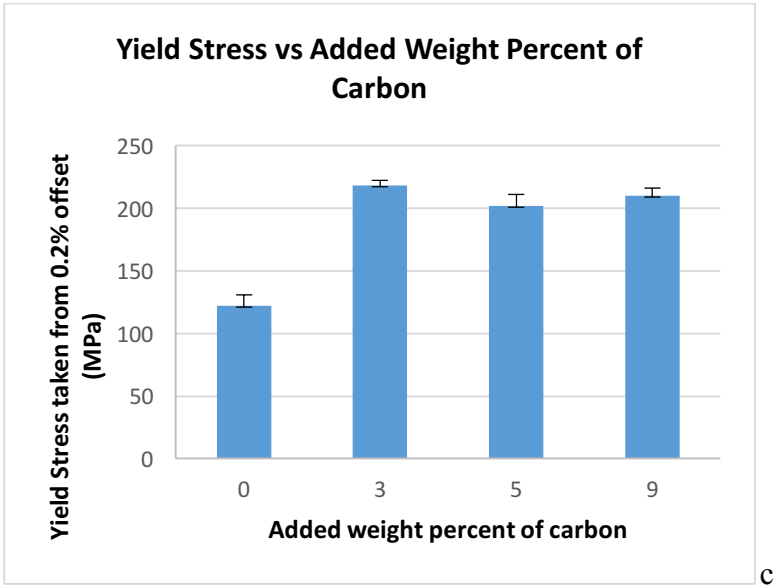

c

Figure 2.3 Elastic modulus(a), yield stress(b), and ultimate tensile stress(c) of copper wires determined by tensile test.

To study the fracture surfaces, SEM images of the fracture surfaces were taken (see Figure 2.4). The SEM images show trans-granular fracture with dimples throughout the fractured areas of all samples. Similar fracture surfaces can be seen in other research, such as the one conducted by Chen [9]. Chen studied polycrystalline copper plates that were processed through cold rolling and annealing subjected to planar impact spalling. The dimples in Chen's research were associated with a microvoid coalescence. Chen also found that varying dimple size was caused by varying grain size of the copper samples. This effect is not seen in the current experiment, suggesting the samples have similar grain size. All samples were processed the same way, thus the addition of carbon does not seem to affect the general fracture surface of the tensile test or grain size. Inclusions can be seen in many dimples as shown in Figure 2.2 b, d, f, and h. Similar inclusions can be seen in SEM fracture surfaces of API X70 steel conducted by Perez [10]. Perez identified the inclusions as metallic, which is expected since they appear similar to the rest of the material in the SEM images. In Figure 2.2 a slight increment in quantity and size of the inclusions appears as the added weight percent of carbon increases. This seems to suggest the clumps of unidentified metallic alloy or oxide form and increase slightly in size and quantity with the addition of carbon. Thus, further analysis is required to identify these agglomerates. The fracture surfaces are also similar to surfaces presented by Shugart [6] in the patent application for covetics. Less magnified SEM images of the fracture areas are presented in Figure 2.5. The samples show necking, characteristic of ductile fracture. The fracture surface of the CuC0, Figure 2.5a, has a notable reduction in the cross section area caused by necking. The CuC9 sample fracture surface, Figure 2.5b, shows only a slight cross-sectional area reduction.

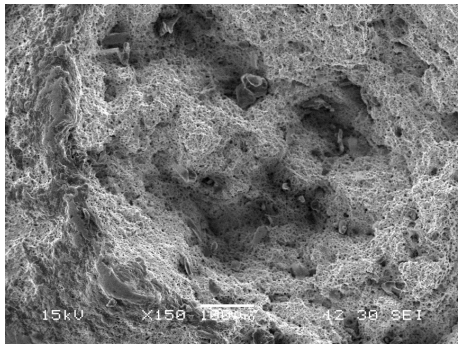

a

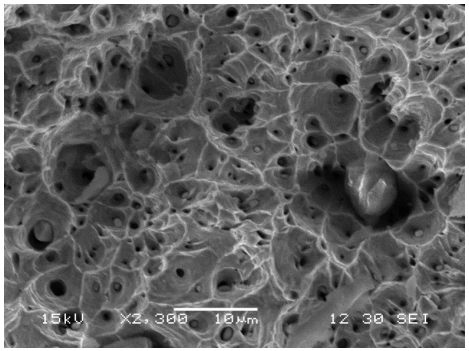

b

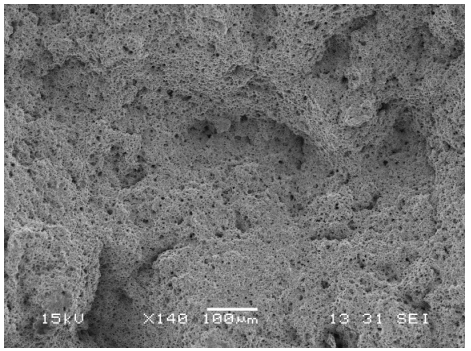

c

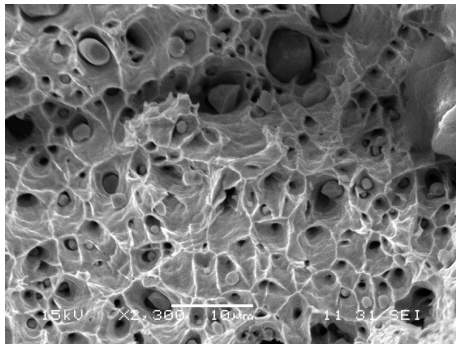

d

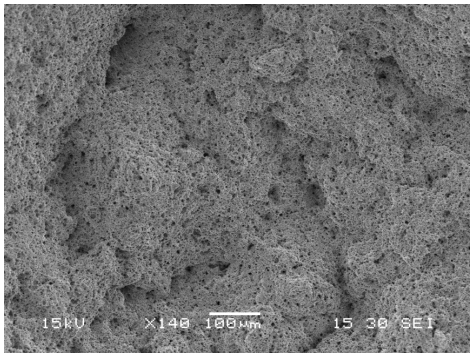

e

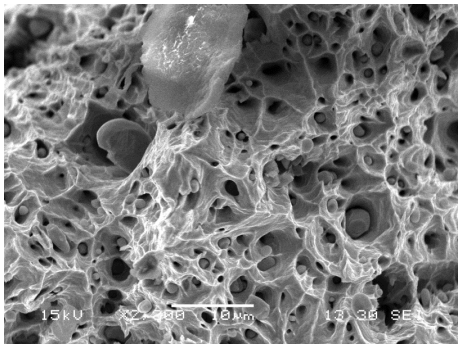

f

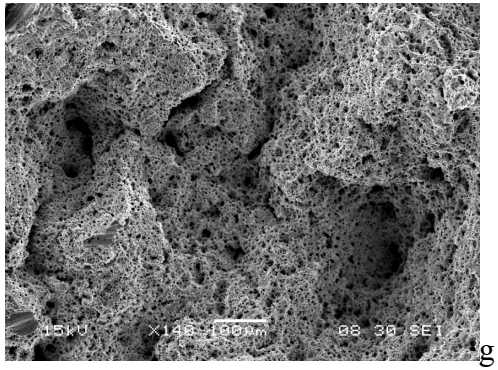

g

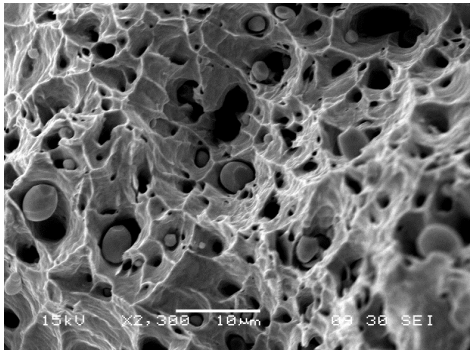

h

Figure 2.4 SEM image of fracture surfaces for the copper wires a) CuC0 150x mag. b) CuC0 2300x mag. c) CuC3 140x mag. d) CuC3 2300x mag. e) CuC5 140x mag. f) CuC5 2300x mag. g) CuC9 140x mag. h) CuC9 2300x mag.

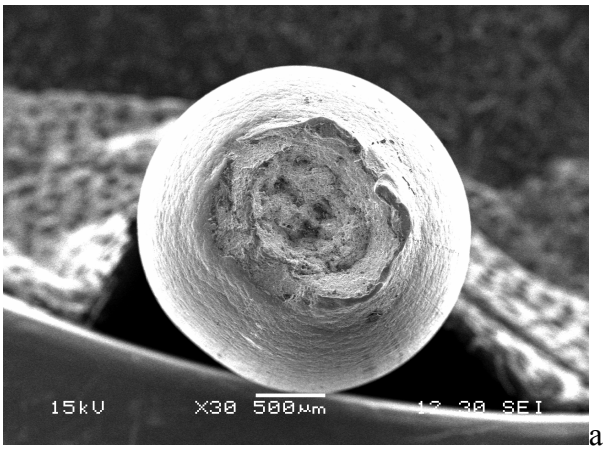

a

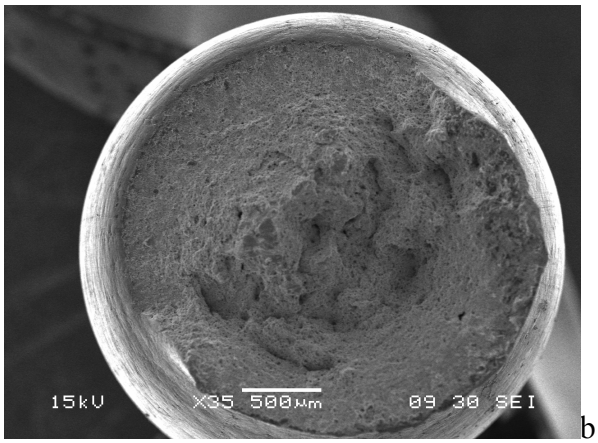

b

Figure 2.5 Fracture surface of a) CuC0 and b) CuC9 covetic for the tensile test.

CHAPTER 3: NANOINDENTATION

3.1 Introduction

Nanoindentation tests can provide hardness and elastic modulus information about a sample while using only a small sample area. A typical loading response for the nanoindenter can be seen in Figure 3.1.

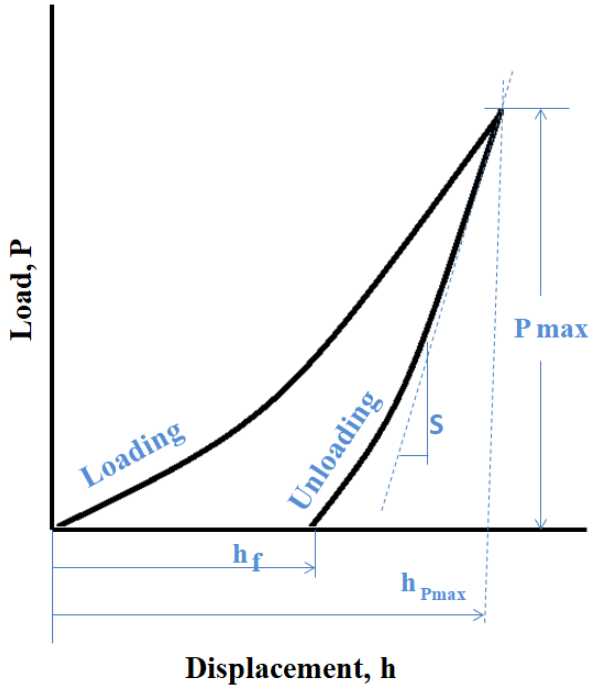

Figure 3.1 Schematic of loading response provided by nanoindenter.

The reduced elastic modulus E_r, which is the elastic modulus of the indenter and the sample together, is expressed as

$$E_r = \frac{S}{\beta}\sqrt{\frac{\pi}{A}} \tag{3.1}$$

where S is the contact stiffness, β is a constant characteristic of the indenter, and A is the area of contact [12]. The elastic modulus of the sample, E_s, is then calculated using Equation 3.2

$$E_s = \frac{1-v_s^2}{\frac{1}{E_r}-\frac{1-v_n^2}{E_n}} \quad (3.2)$$

where v_s is the Poisson's ratio of the sample, v_n is the Poisson's ratio of the nanoindenter, E_n is the elastic modulus of the nanoindenter. The hardness can be calculated by using Equation 3.3

$$H = P_{max}/A \quad (3.3)$$

where P_{max} in the maximum load and A is the area of contact [12][13].

When nanoindentation is performed, the material may deform and create a pile up. The pile-up will generate more contact area between the indenter and the sample. This extra area needs to be calculated in order to find the corrected hardness and corrected elastic modulus of the measured samples. The total area, A_{total}, will be the area of the indentation and the area of the pile-up.

$$A_{total} = A_{OP} + A_{PU} \quad (3.4)$$

where A_{OP} is the Oliver-Pharr area and A_{PU} is the pile up area. The pile up area can be calculated using the Equation 3.5

$$A_{PU} = \frac{\pi\, b_{average}}{4} \sum_{i=1}^{3} a_i \quad (3.5)$$

where $b_{average}$ is the average length of the sides of the triangle generated by the indentor, a_i is the height of the pileup section [14].

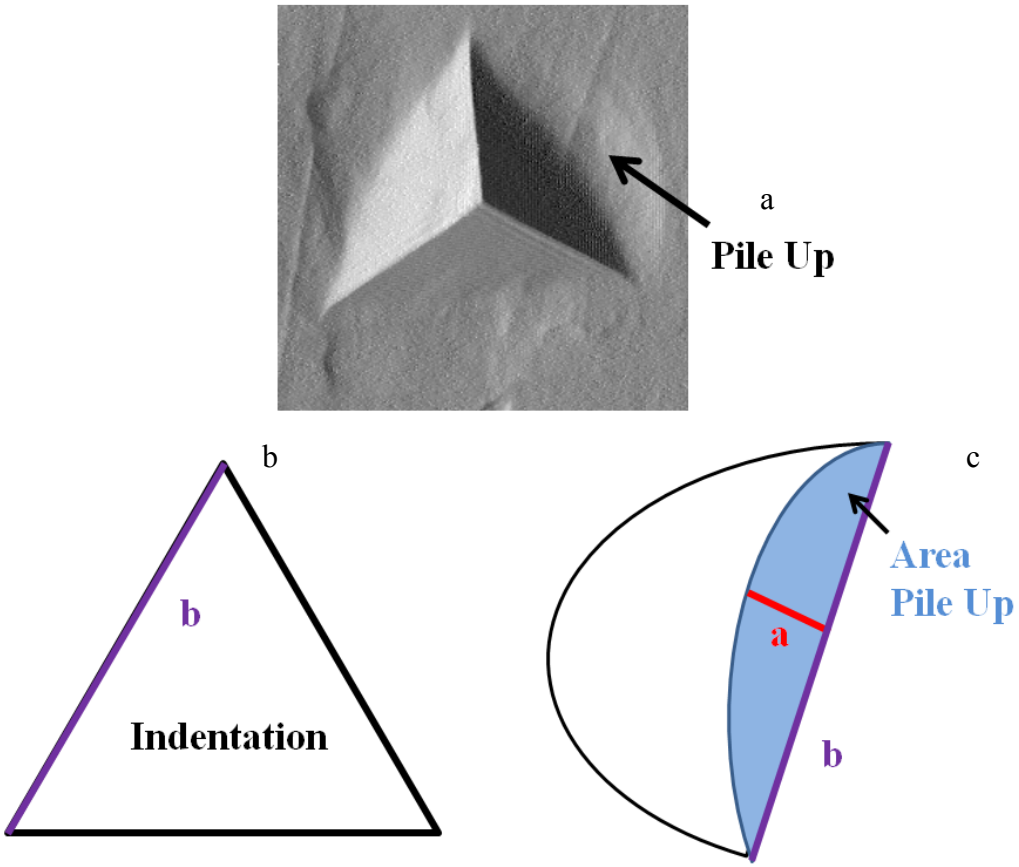

Figure 3.2 Picture and diagram of nanoindentation pile up: a) AFM image of nanoindentation of CuC3 covetic sample with pile-up present, b) diagram of length b of triangle indentation created by nanoindentation c) diagram of pile-up height, area, and length b.

3.2 Method

Since a flat surface is preferred in order to perform nanoindentation, the samples were embedded in an epoxy. The epoxy was made from a two mixture formula. The first part of the mixture, Mix A, consists of 5g of Glycerol polyglycidyl ether known as LX-112 resin (Ladd Inc., Williston, Vermont) and 6.4 g of Dodecenylsuccinic anhydride ($C_{16}H_{26}O_3$) known as DDSA (Ladd Inc., Williston, Vermont). The second part of the mixture, Mix B, consists of 7.5 g LX-112 and 6.75 g of Methyl nadic anhydride ($C_{10}H_{10}O_3$) known as NMA (Ladd Inc., Williston,

Vermont). Both parts were individually mixed using a wooden stick to combine the ingredients. To create the final mixture 1.7 g of the Mix A, 11.7g of Mix B, and 0.23 mL of Tri(dimethylaminomethyl) phenol ($C_{15}H_{27}N_{3O}$), known as DMP-30, were mixed at a temperature of 80^{o}C. The mixture was then put into silicone molds with pieces of the wires, one wire piece per mold. Once the epoxy was solid, presented in Figure 3.3, a grinding and polishing process was performed.

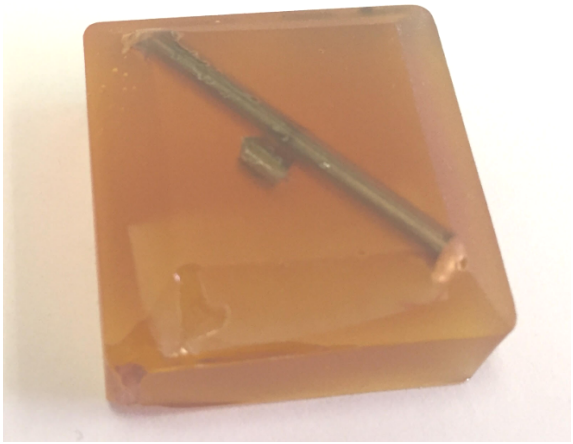

Figure 3.3 Unpolished copper wire sample embedded in epoxy.

The embedded samples were polished using a MetaServ 250 Grinder-Polisher (Illinois Tool Works Inc, Lake Bluff, Illinois) with sand paper of 320, 400, 800, and 1200 grit. Once a flat surface is obtained the samples were then polished using a polish cloth and 0.05 μm gamma alumina solution (Illinois Tool Works Inc, Lake Bluff, Illinois).The polishing was continued until the samples showed minimal scratches and a mirrorlike surface.

To perform the nanoindentation, the TI 950 Triboindentor (Hysitron, Minneapolis, Minnesota) was used. Before the nanoindentation test, the nanoindenter was calibrated using a quartz sample and a 40 segment quasi-static partial unload load function, as seen in Figure 3.4.

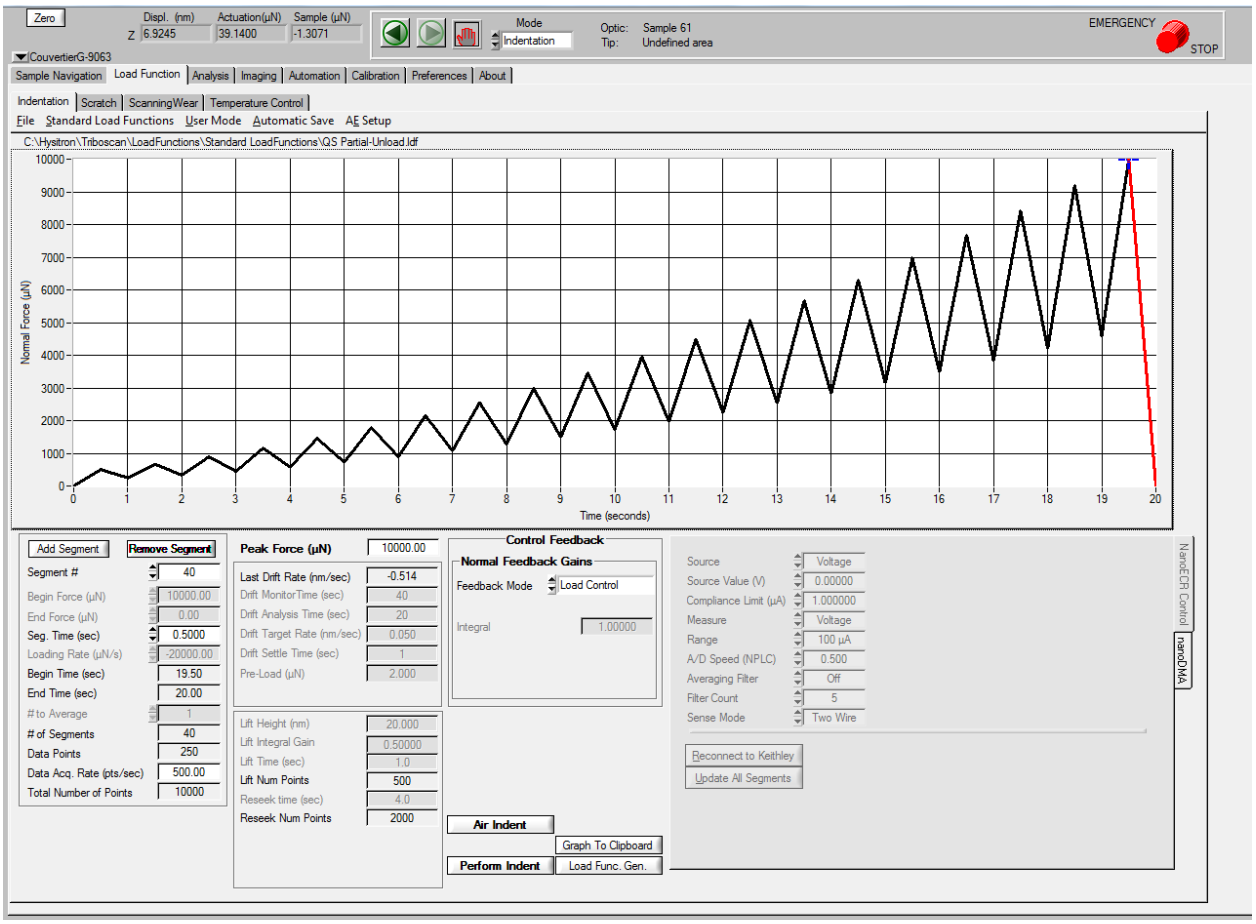

Figure 3.4 Quasistatic partial unload load function used in calibration test of nanoindenter.

The results were then used to calculate the contact area via a five constant equation seen in Equation 3.6. By modifying Equation 3.6, the results of the calibration nanoindenter test can be modified to accurately provide the elastic modulus and hardness of the quartz sample, and later of the test samples.

$$A = C_1 h^2 + C_2 h - C_2 h^{1/2} + C_3 h^{1/4} - C_4 h^{1/8} \quad (3.6)$$

where C_1, C_2 , C_2 ,C_3 ,C_4 are constant derived from the quartz calibration test and h is the displacement. A nine-point (nine indentations) test with a 20um spacing between indents was conducted on one sample of each weight percent of added carbon for each of the maximum loads. The test was conducted using a diamond Berkovich tip. The quasi-static load function had

a 10-second ramp up from a zero load to the maximum load, 10-second hold at the maximum load, and 10-second ramp down from the maximum load to a zero load, as shown in Figure 3.5. The test was conducted with two different maximum applied loads, 5,000 uN and 10,000 uN. To find the sample elastic modulus the following constant values were used: E_n of 1140 GPa, v_s of 0.3, and v_n of 0.07 [15].

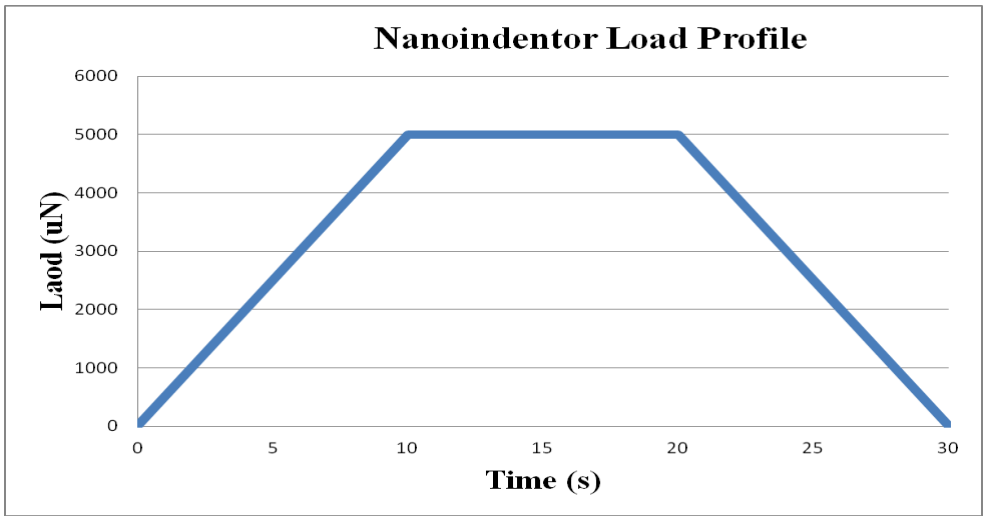

Figure 3.5 Quasi-static load function used in nanoindentation test.

To correct for pileup, Atomic Force Microscope (AFM) images were taken using the nanoindentor. The AFM had a setpoint of 2uN, 1 scanpass of 256 seconds at 1 Hz. The AFM images were taken before and after the nanoindentation to more accurately measure the pile ups from the indentation. The corrected hardness and elastic modulus of the samples were calculated and the values are presented as averages and standard deviations.

3.3 Results and Discussion

The 0, 3, 5, and 9 added weight percent of carbon samples were tested using the nanoindenter. The results of the nanoindentation test at a maximum load of 5,000uN can be seen in Table 3.1, Figure 3.6 and Figure 3.7. The highest hardness is found in the CuC0 sample with a value of 2.1 GPa, followed closely by the CuC3 sample with 1.9 GPa. The CuC5 and CuC9

had lower hardness values of 1.6 GPa and 1.3 GPa, respectively. Thus, as the carbon content increases the hardness decreases. The elastic modulus showed a different behavior, being CuC5 the highest elastic modulus with a value of 134 GPa. The CuC0 sample has a 122 GPa elastic modulus, CuC3 had 102 GPa, and CuC9 52 GPa. The CuC0, CuC3 and CuC5 showed elastic modulus values consistent with the elastic modulus of copper shown in Table 1.2.

Table 3.1. Quasi-static nanoindentation hardness and elastic modulus at maximum load of 5,000 uN.

Value		CuC0	CuC3	CuC5	CuC9
Hardness (GPa)	Average	2.10	1.99	1.69	1.38
	Standard Deviation	0.36	0.42	0.09	0.11
Elastic Modulus (GPa)	Average	122.9	102.2	134.2	52.69
	Standard Deviation	12.7	2.3	7.4	4.1

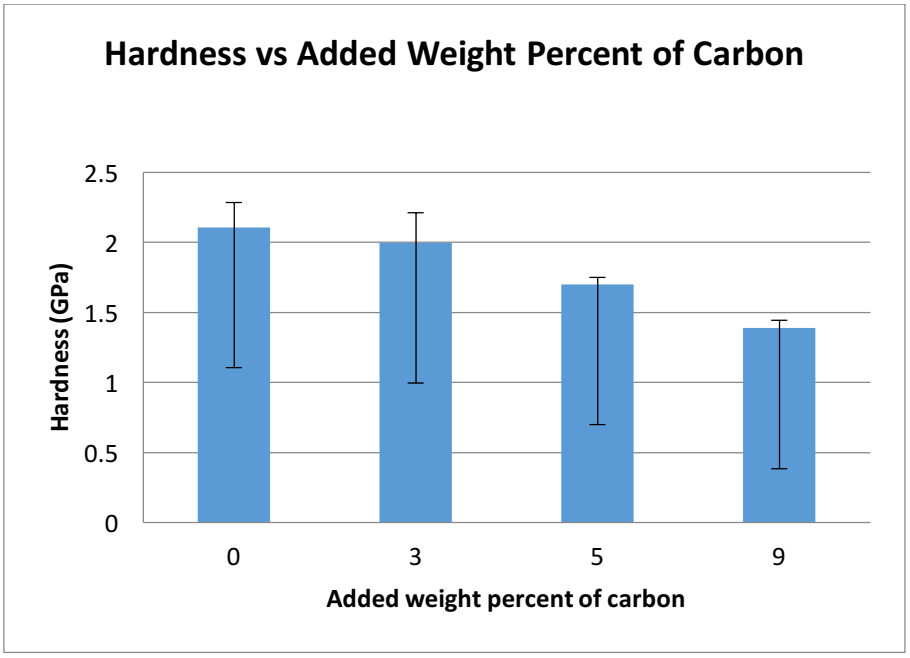

Figure 3.6 Hardness versus added weight percent of carbon results from nanoindentation test at maximum load of 5,000 uN.

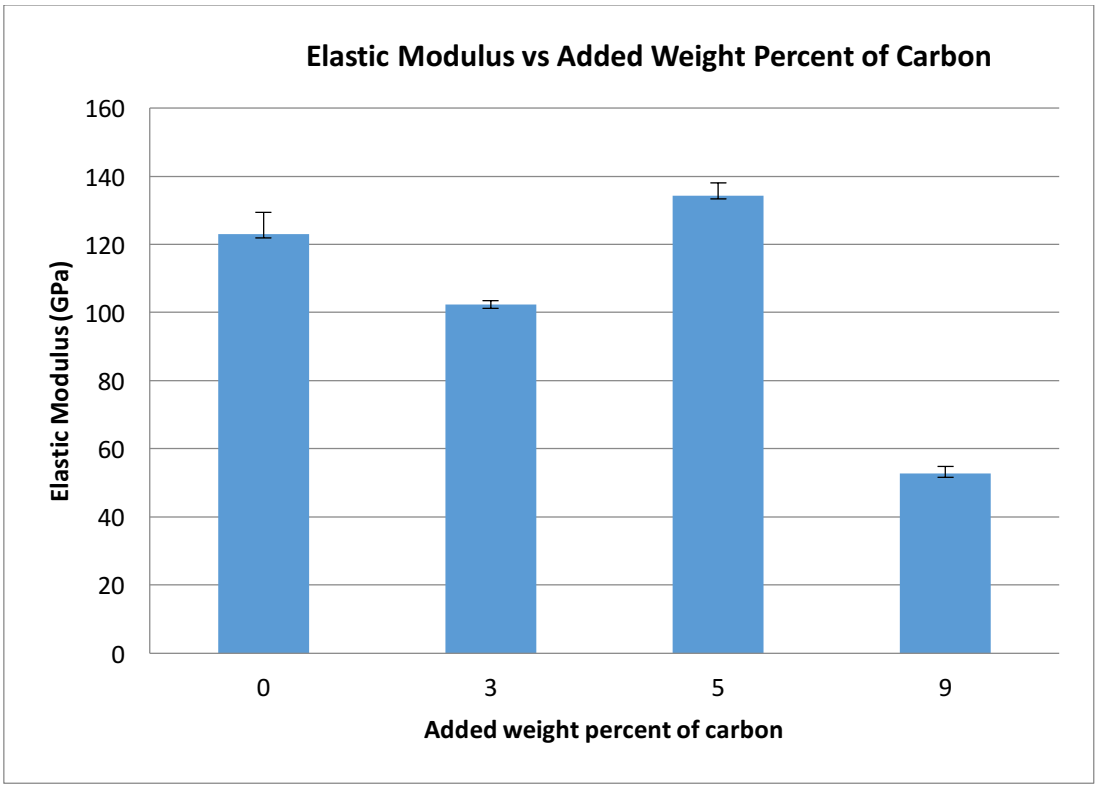

Figure 3.7 Elastic modulus versus added weight percent of carbon results from nanoindentation test at maximum load of 5,000 uN.

The results of the nanoindentation test at a maximum load of 10,000uN can be seen in Table 3.2, Figure 3.8, and Figure 3.9. The highest mean hardness at this higher load is found in the CuC5 sample with a value of 2.1 GPa. The CuC0 and CuC3 samples had mean hardness values of of 1.6 GPa each, and CuC9 had a hardness value of 1.5 GPa. The elastic modulus showed a different behavior from the lower maximum load, namely the CuC0 sample gave highest elastic modulus with a value of 127 GPa. The CuC3 sample had a 66 GPa elastic modulus. The CuC5 sample had an elastic modulus of 102 GPa. Once more the CuC9 sample had the lowest value for elastic modulus with a value of 55 GPa. Such a low value for the CuC9 in both maximum loads may be caused by the nanoindenter indenting a section with a low carbon content.

Table 3.2 Quasi-static nanoindentation hardness and elastic modulus at maximum load of 10,000 uN.

Value		CuC0	CuC3	CuC5	CuC9
Hardness (GPa)	Average	1.6	1.6	2.1	1.5
	Standard Deviation	0.1	0.1	0.4	0.1
Elastic Modulus (GPa)	Average	127.3	66.5	102.3	55.5
	Standard Deviation	2.3	3.4	3.2	2.5

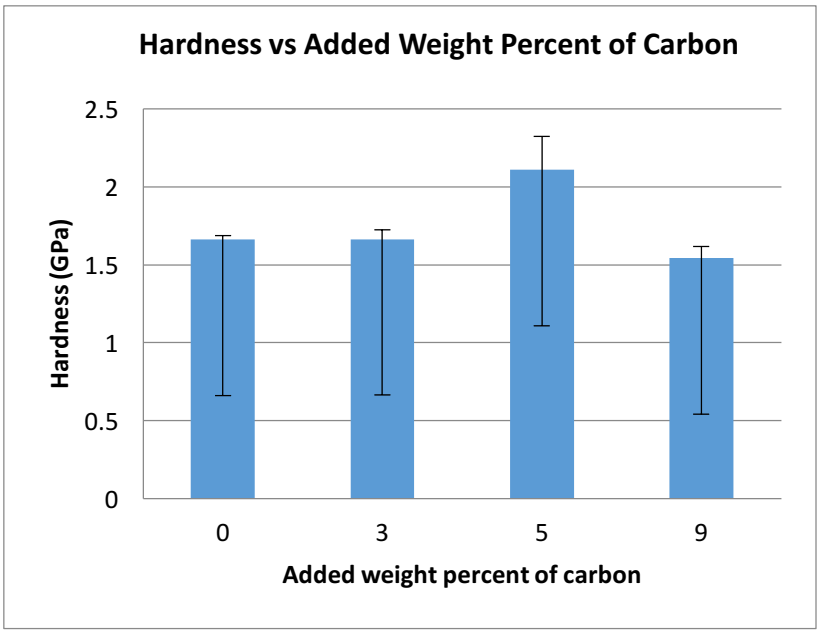

Figure 3.8 Hardness versus added weight percent of carbon results from nanoindentation test at maximum load of 10,000 uN.

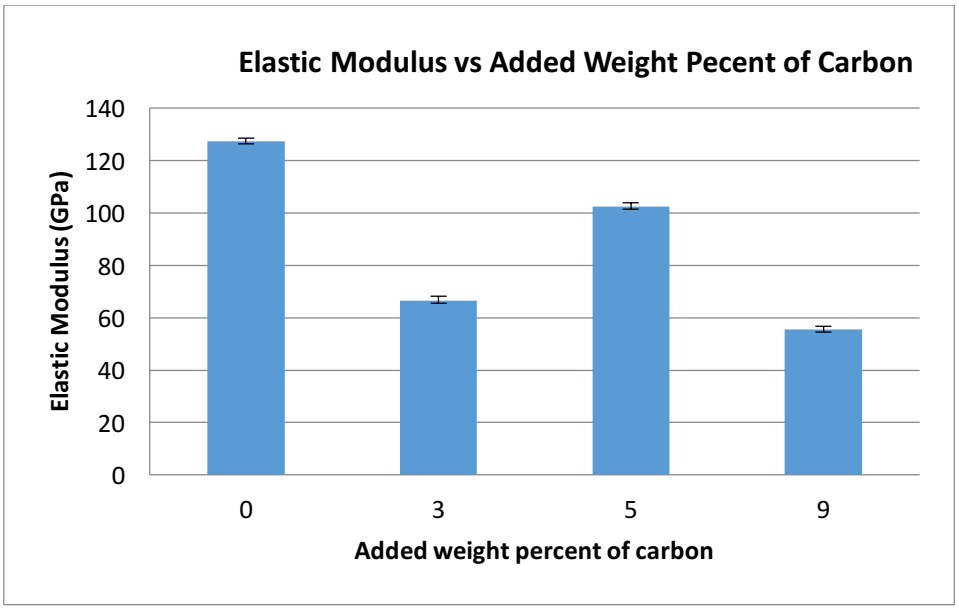

Figure 3.9 Elastic modulus versus added weight percent of carbon results from nanoindentation test at maximum load of 10,000 uN.

The results of the nanoindentation test show a dependence with the maximum applied load. With an increase maximum load, the CuC0 and CuC9 samples showed an increase in elastic modulus value while the other samples exhibited decreased elastic modulus. The hardness results for the CuC5 and CuC9 increased while the others decreased with the increase of maximum load. Thus, adding carbon tends to increase the hardness but slightly decrease the elastic modulus as the load increases. Comparing the 5,000 uN maximum load values with previously reported values of copper covetics [16], the behaviors differ. The material used in Valdez [16] was Cu 10200-based as cast covetics with same reported carbon contents (0, 3, 5, and 9 wt%C). In this previous research, the CuC9 sample had the highest value of elastic modulus followed by CuC3, CuC0, and CuC5. The current test results from highest to lowest were CuC5, CuC0, CuC3, and CuC9. The hardness in Valdez research, going from highest to lowest, were CuC9, CuC3, CuC5, CuC0. This is almost the reverse of the current research, from highest to lowest, CuC0, CuC3, CuC5, and CuC9. The general values of the elastic modulus and

hardness were also higher in the current research. These differences may be due to differences in processing and post-processing of samples as well as local variations in carbon content resulting in local differences in properties.

CHAPTER 4: MICROINDENTATION

4.1 Introduction

Hardness tests measure the resistance of a material to deformation caused by an indenter. Microindentation is similar to the more commonly known Vickers hardness test, but with lower applied loads. Microindentation tests are commonly used in small samples or when different phases are found in a single sample. To find the hardness, the dimensions of the indentation and the applied load are used in Equation 4.1 [11]

$$HV_{mass} = \frac{1854.4\ P}{(d_1\ d_2)^2} \tag{4.1}$$

where *mass* is the numerical value of the load or mass applied, P is the load, and d_1 and d_2 are the dimensions of the indentation as presented in Figure 4.1.

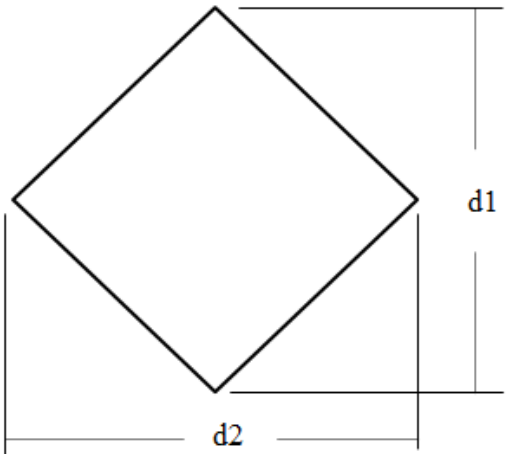

Figure 4.1 Dimensions of the microindentation used for calculations of hardness.

4.2 Method

The microindentation test was performed on one copper sample for each weight percent of added carbon. Each sample was indented eight times and an average was calculated. The samples used were embedded in epoxy and polished, as previously described in Chapter 3. The

microindenter used to conduct the test is the Microindentor Hardness Tester (Leitz Wetzlar, Germany), which measures Vickers Knoop hardness. Microhardness was performed with a 500 Pond load. Once the load was applied, the indentations were measured. The hardness average and standard deviation is calculated and reported for every sample.

4.3 Results and Discussion

The results of the microindentation test can be found in Table 4.1 and Figure 4.2. The sample with the highest hardness value was the CuC3 with an HV_{500} value of 117.9 kp/mm^2 , followed closely by CuC9 with a microhardness of 117.1 kp/mm^2. The CuC5 and CuC0 had lower values of 113.4 kp/mm^2 and 113.7 kp/mm^2 respectively. The highest hardness reported for the current research was for the CuC3 sample which following CuC9, CuC0 and CuC5.

Khisamov [17] tested the microhardness of copper composites with carbon reinforcements at 0, 2, 3, and 4 weight percents of added carbon. The highest to lowest hardness went pretty much in the same order as highest to lowest added weight percent of carbon. Novac et al [18] saw similar behavior in the electrodeposited copper carbon with varying dispersion baths. Novac found that the microhardness of copper carbon composite layer reduced with the addition of graphene in the disperse phase, increase for an 80% dispersion bath but was less than for pure copper. Thus, the addition of carbon generally increased the microhardness of the composite sample.

Table 4.1 Microhardness copper wire hardness HV500.

Value		CuC0	CuC3	CuC5	CuC9
HV 500 (kp/mm^2)	Average	113.7	117.9	113.4	117.1
	Standard Deviation	3.6	4.0	3.8	2.5

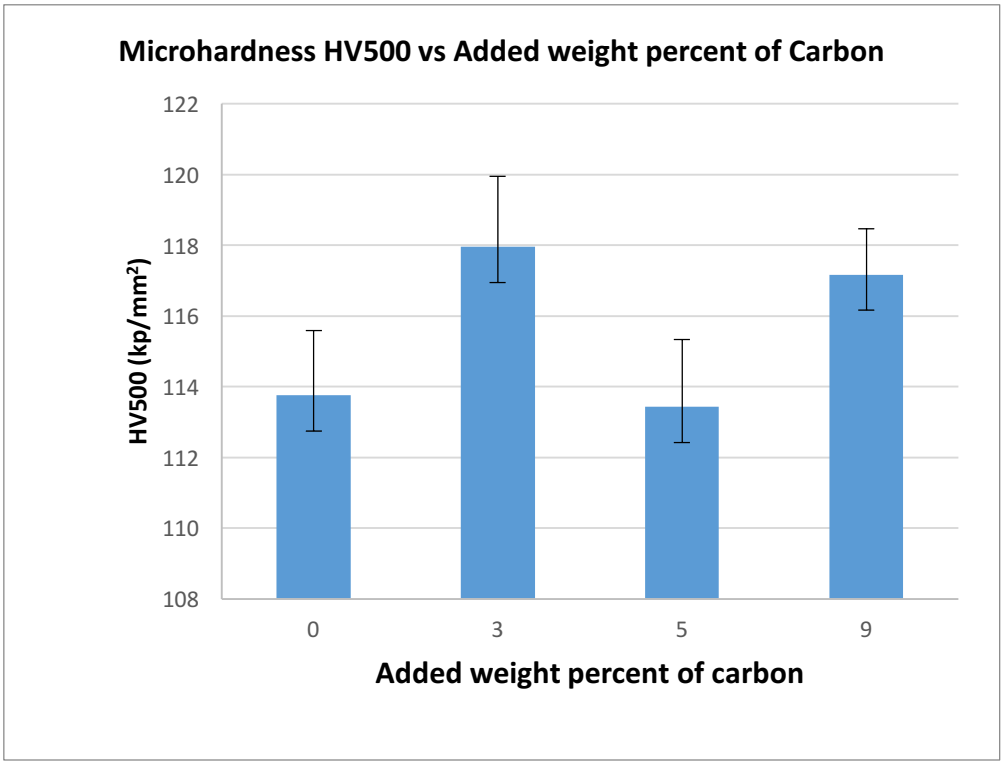

Figure 4.2 Microhardness results for copper samples with different weight percent of added carbon.

CHAPTER 5: TRANSMISSION ELECTRON MICROSCOPY

5.1 Introduction

Transmission electron microscopy (TEM) is used to take diffraction patterns as well as magnified images of thin samples. TEMs use accelerated electrons and detectors to collect the images of samples inside a vacuum [19]. In a TEM, electrons are passed through a condenser lens, an electromagnetic lens, to focus the electrons. The focused electrons will then travel to the sample and either transverse the sample or be diffracted. The beams that are transmitted travel through an objective lens in order to show an image of the sample. The beams that pass through the sample and travel with the same direction will focus on the same area in the back focal plane and generate a diffraction pattern of the sample [20]. If the sample is thin enough the TEM can easily detect individual grains and the orientation of the atoms. The TEM diffraction patterns are able to present other information about the sample such as crystalline structure and lattice parameters.

To find the lattice parameter of a crystalline structure, the Bragg's law, Equation 5.1, is one of the principal equations used

$$2d \sin \Theta_b = n \lambda \tag{5.1}$$

In Equation 5.1, d is interplanar distance spacing, Θ_b is the Bragg's angle which is the angle between the incidence ray and the surface of the sample, n is an integer, λ is the wavelength of the incident plane wave.

5.2 Method

Only one sample, CuC9, was tested using the TEM. The CuC9 sample was prepared using a Dual-Beam Focus Ion Beam (FIB) System DB235 (Field Electron and Ion Company,

Hillsboro, Oregon). To prepare the sample, a protective layer of platinum is deposited over an area of 10 um x 5 um for a height of approximately 3 um. This is done to protect the sample and help a uniform thinning. A 10 um x 5 um x 10 um piece was cut out of the main CuC9 sample by using the ion beam. The small piece was then thinned by exposing the sample to an ion beam while decreasing the aperture from 1000pA to 50pA. This was performed at a voltage setting of 30kV until the sample had a thickness of around 100nm. The thinned sample was placed in a copper TEM holder using platinum deposition. Polishing steps were then performed on both faces of the sample using the ion beam with a 100pA aperture at 5kV. TEM images were taken using JEOL-2010 TEM with a LaB_6 filament (JEOL, Akishima, Tokyo, Japan). The TEM images and diffraction patterns were taken at 200kV with a 20cm camera length, and a wavelength of 0.0251 A.

5.3 Results and Discussion

The TEM images in Figure 5.1 are from various locations of the CuC9 sample. Multiple grains can be seen in Figure 5.1a, b,c, and d. The sizes of the grains vary and have defined thin grain boundaries. Figure 5.1c shows dislocation inside a grain. The images in Figure 5.1 show dislocations on the grain boundariesOn Figure 5.1 a and c some grains seem to have "layer or strips" of dark and light areas. This may be because the grains are formed by layers of copper with varying carbon content.

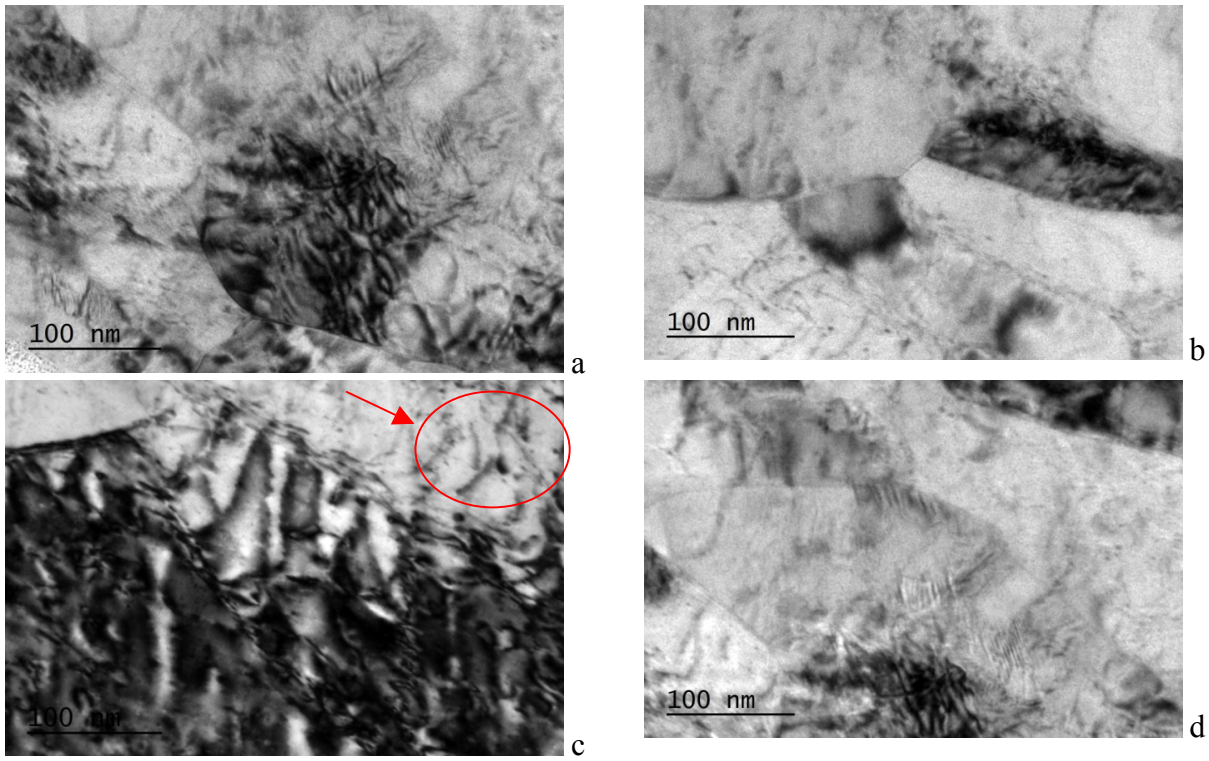

Figure 5.1 TEM images of CuC9 showing multiple grains and dislocations.

Figure 5.2 and Figure 5.3 show TEM images at different locations in the CuC9 TEM sample. The image on the right are the diffraction pattern of the section imaged on the left. On Figure 5.2 a and c and Figure 5.3 a and c, Moire fringes can be appreciated through the TEM image. Moire fringes are caused by interference from multiple semitransparent materials [21]. The interference could be explained by the overlapping of copper and carbon layer. Carbon will have a different lattice parameter than the copper which could cause a fringe in the image.

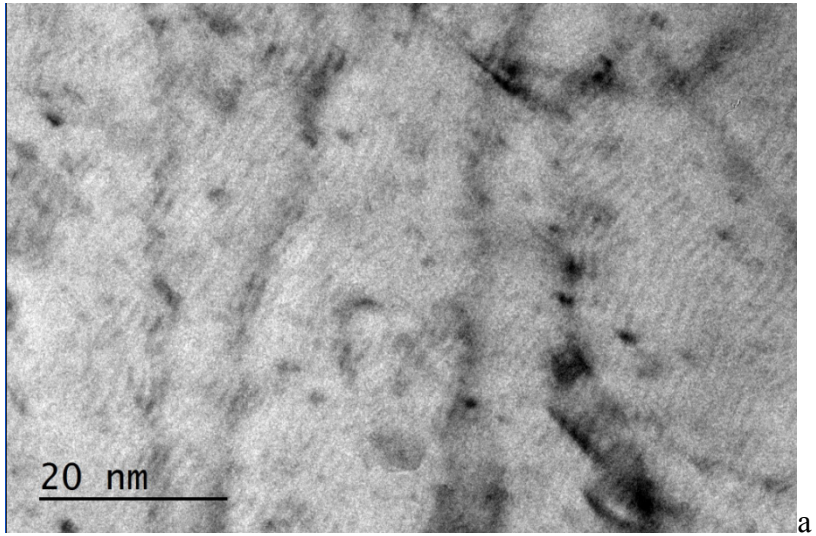

a

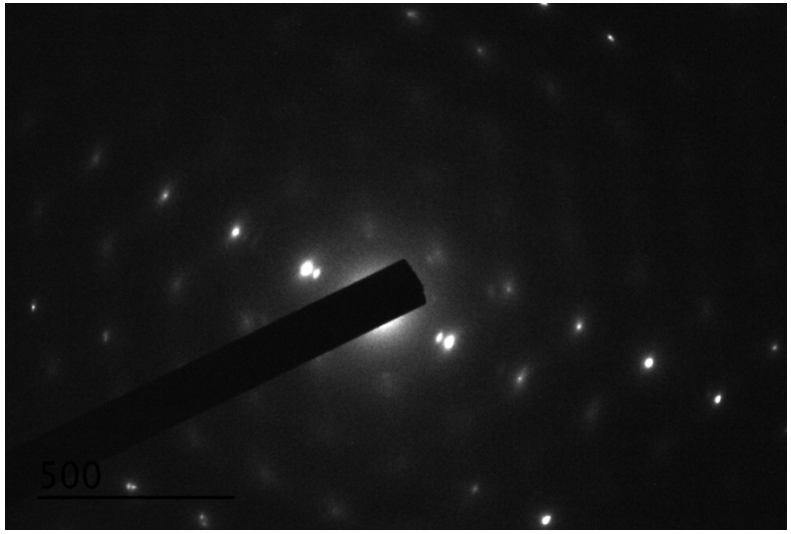

b

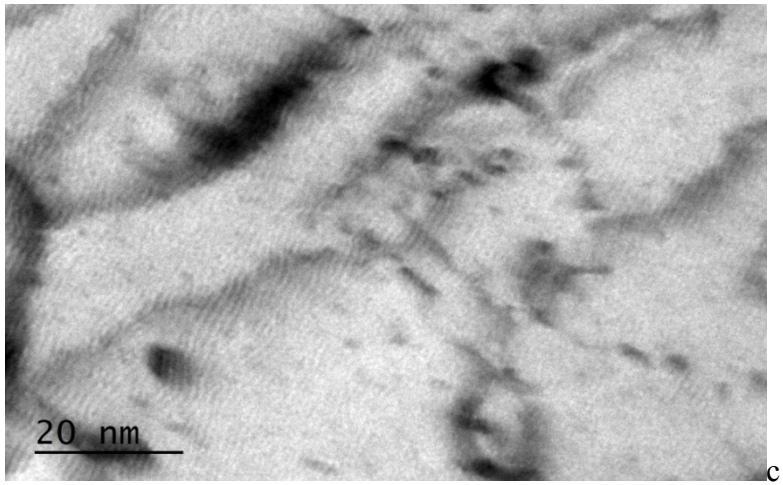

c

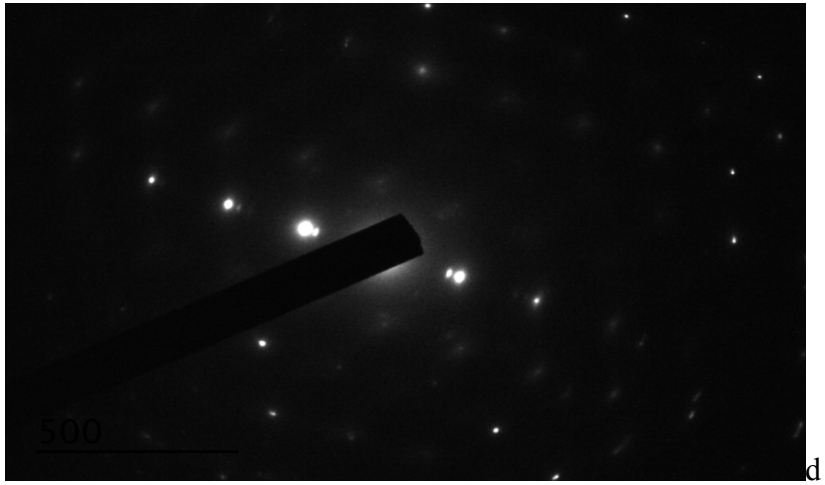

d

Figure 5.2 TEM images at high magnification show of the CuC9 sample Moire fringes throughout the image and double spots in the diffraction pattern.

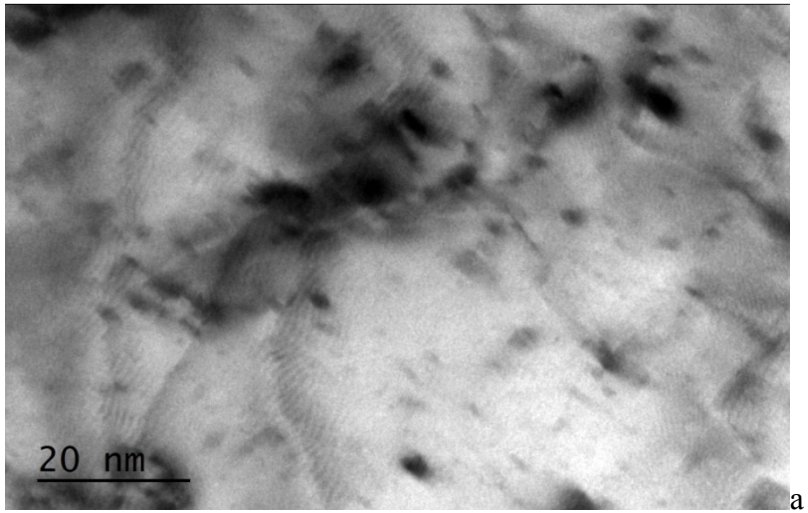

a

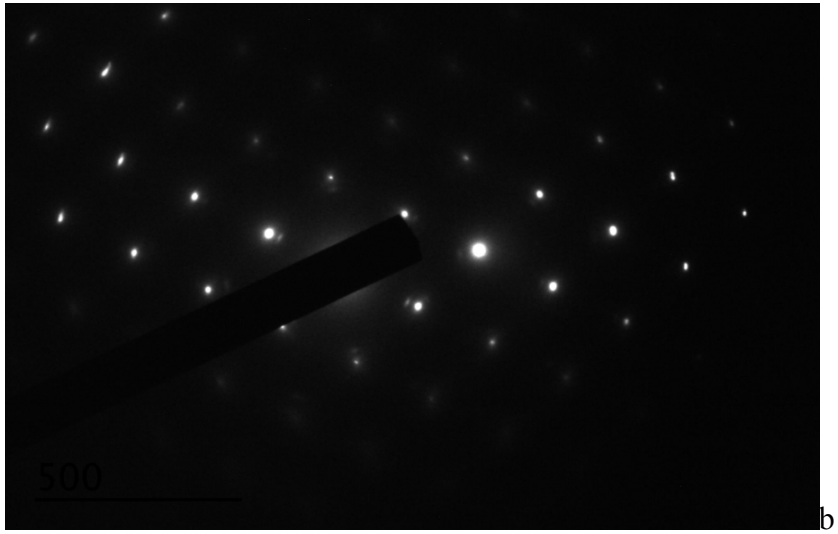

b

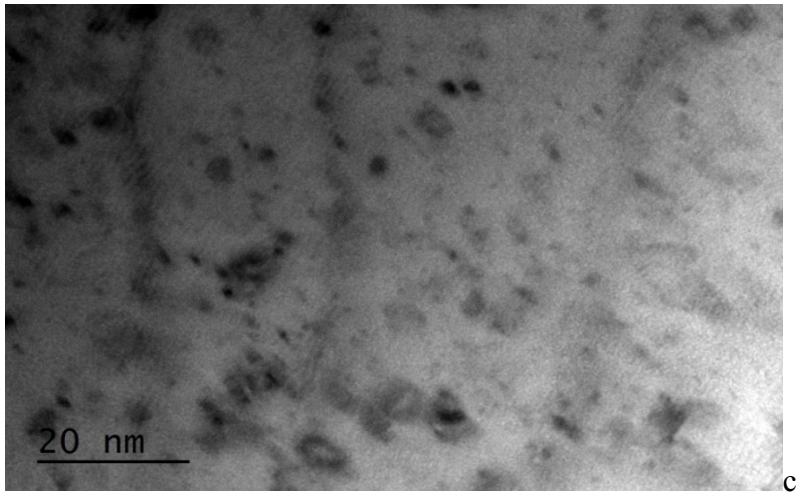

c

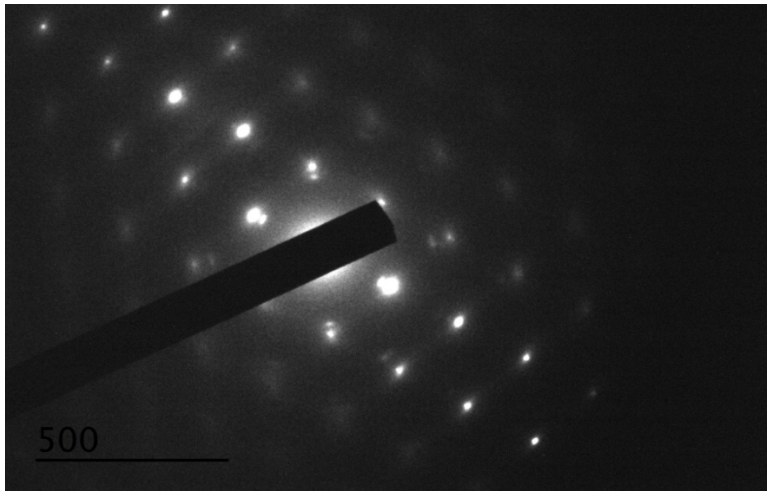

d

Figure 5.3 TEM images at high magnification show of the CuC9 sample Moire fringes throughout the image and double spots in the diffraction pattern.

In the diffraction pattern, Figure 5.2 b and d and Figure 5.3 b and d, it is clear that the copper covetic sample has a face center cubic crystalline structure. The arrangement of the diffraction pattern is as seen in Figure 5.4 [20]. The diffraction patterns show double dots in some location. This is probably caused by the carbon diffraction pattern being imposed into the stronger copper diffraction pattern.

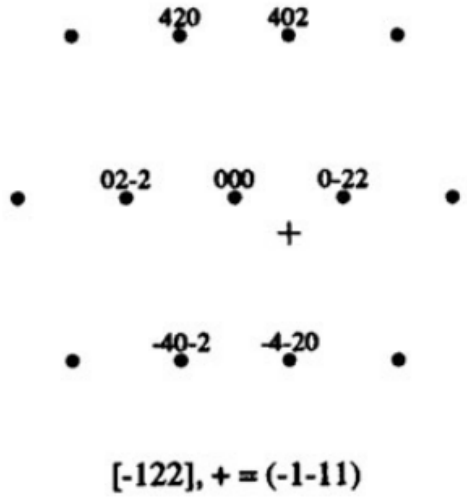

Figure 5.4 Possible diffraction pattern for face center cubic material which is concurrent with the CUC9 sample diffraction patterns. ***Taken from Advanced transmission electron microscopyimaging and diffraction in nanoscience [20].***

CHAPTER 6: CONCLUSIONS

Copper samples with varying added weight percentages of carbon were tested using tensile test, nanoindentation, microindentation, and TEM. The results were averaged with respect to each sample for each test. With respect to the tensile test, the addition of carbon increased the yield stress and ultimate tensile stress. The elastic modulus increased slightly with the addition of carbon, yet all values of elastic modulus were small in comparison to other copper alloys. It is important to note the test was performed in a non-standard format due to the fabrication limitation of the copper covetics. The strain at the moment of fracture decreases when carbon was added. Thus, the addition of copper increased the strength but made the samples less elastic. In the nanoindentation test, the elastic modulus and the hardness tended to be less for the CuC3, CuC5 and CuC9 samples than the CuC0 sample when the test was performed with a 5,000uN maximum load. This can be caused by the nanoindenter indenting sections with higher carbon content. Only the hardness for a maximum load of 10,000uN tended to be equal to the CuC0 sample. The microindenter hardness results were also similar for all samples. A comparison between the samples can be seen in Table 6.1, where the sample numerical result for a particular test measurement or property was divided by the value of the CuC0 sample. The TEM results show the possibility of the carbon being incorporated into the copper.

Future work may include analyzing the chemical composition of the samples. Such analysis includes analyzing the agglomerates seen on the fracture surfaces, to correctly see the composition of such objects. Such analysis would also help identify the actual amount of carbon inside the covetics. This has proven difficult due to challenges in measuring carbon content using existing experimental techniques. Additional future work may also include measurement of

electrical properties of copper covetics. Such analysis should reveal if the increase in strength happens without the normal decrease in electrical properties that is associated in copper alloys.

Table 6.1 Comparison between sample and CuC0 result for various test and properties.

Measurement	CuC0	CuC3	CuC5	CuC9
Tensile Test				
Elastic Modulus	1	1.08	1.01	1.07
UTS	1	1.51	1.47	1.53
Yield Stress	1	1.78	1.65	1.72
Fracture Strain	1	0.06	0.06	0.06
Nanoindentor 5,000uN max force				
Elastic Modulus	1	0.83	1.09	0.43
Hardness	1	0.95	0.80	0.66
Nanoindentor 10,000uN max force				
Elastic Modulus	1	0.52	0.80	0.44
Hardness	1	1	1.27	0.93
Microindentor				
Microhardness	1	1.04	1	1.03

REFERENCES

[1] Campbell, F. C. (Ed.). (2008). *Elements of metallurgy and engineering alloys.* Materials Park, Ohio: ASM International.

[2] Mendenhall, J. H. (Ed.). (1977). *Understanding copper alloys: The manufacture and use of copper and copper alloy sheet and strip*. East Alton, Illinois: Olin Brass.

[3]Davis, J. R. (Ed.). (1997). *Concise metals engineering data book*. Materials Park, Ohio: ASM International.

[4] Guiderdoni, Ch., Estournès, C., Peigneya, A., Weibela, A., Turqa, V., & Laurent, Ch. (2011). The preparation of double-walled carbon nanotube/Cu composites by spark plasma sintering, and their hardness and friction properties. *Carbon,* 49(13), 4535-4543.

[5] Ullbrand, J. M., Córdoba, J. M., Tamayo-Ariztondo, J., Elizalde, M. R., Nygren, M., Molina-Aldareguia, J. M., & Odén, M. (2010). Thermomechanical properties of copper–carbon nanofibre composites prepared by spark plasma sintering and hot pressing. *Composites Science & Technology*, 70(16), 2263-2268. doi:10.1016/j.compscitech.2010.08.016

[6] Shugart, J. V., & Scherer, R. C. (2014). U.S. Patent No. 8647534. Washington, DC: U.S. Patent and Trademark Office.

[7] Salamanca-Riba, L. G., Isaacs, R. A., LeMieux, M. C., Wan, J., Wuttig, M., Kuklja, M. M., & ... Santiago, J. R. (2015). Synthetic alloys: synthetic crystals of silver with carbon: 3d epitaxy of carbon nanostructures in the silver lattice. *Advanced Functional Materials*, 25(30), 4746. doi:10.1002/adfm.201570202

[8] Isaacs, R. A., Zhu, H., Preston, C., Mansour, A., LeMieux, M., Zavalij, P. Y., & ... Salamanca-Riba, L. G. (2015). Nanocarbon-copper thin film as transparent electrode. *Applied Physics Letters*, 106(19), 1-5. doi:10.1063/1.4921263

[9] Chen, T., Jiang, Z. X., Peng, H., He, H. L., Wang, L. L., & Wang, Y. G. (2015). Effect of grain size on the spall fracture behavior of pure copper under plate-impact loading. *Strain*, 51(3), 190-197. doi:10.1111/str.12132

[10] Pérez Campos, R., Contreras Cuevas, A., & Esparza Muñoz, R. A. (Eds.). (2017). *Characterization of metals and alloys*. Switzerland: Springer.

[11] Smithells, C. J., Gale, W. F., & Totemeier, T. C. (2004). *Smithells metals reference book*. Amsterdam: Elsevier Butterworth-Heinemann.

[12] Oliver, W., & Pharr, G. (2010). Nanoindentation in materials research: Past, present, and future. *Material Research Society Bulletin*, 35(11), 897-907. doi:10.1557/mrs2010.717

[13] Oliver, W., & Pharr, G. (1992). An improved technique for determining hardness and elastic modulus using load and displacement sensing indentation experiments. *Journal of Materials Research*, 7(6), 1564-1583. doi:10.1557/JMR.1992.1564

[14] Kese, K., Li, Z., & Bergman, B. (2005). Method to account for true contact area in soda-lime glass during nanoindentation with the Berkovich tip. *Materials Science & Engineering*: A, 404(1/2), 1-8. doi:10.1016/j.msea.2005.06.006

[15] Fisher-Cripps, A. C. (2011). *Nanoindentation*. (2011). (3rd ed.). New York, New York: Springer.

[16] Valdez, M. A. (2015). *Nanoindentation of copper covetics and mechanical testing and microstructural imaging of additive manufactured inconel 718*. M.S. thesis, Department of Mechanical Science and Engineering, University of Illinois, Urbana, Illinois.

[17] Khisamov, R., Nazarov, K., Zubairov, L., Nazarov, A., Mulyukov, R., Safarov, I., & ... Huan, N. (2015). Fabrication, microstructure, and microhardness of copper composites

reinforced by carbon nanotubes. *Physics of the Solid State*, 57(6), 1206-1212. doi:10.1134/S1063783415060177

[18] Novac, R., Mihaela Cantaragiu, A., Stancioiu, A., Mitoseriu, O., & Cârâc, G. (2011). Structure and microhardness of the electrodeposited copper-graphite composite layers. *Annals of The University Dunarea De Jos Of Galati: Fascicle II, Mathematics, Physics, Theoretical Mechanics*, 34135-140.

[19] Stolojan, V. (2015). *Nanometrology using the transmission electron microscope*. San Rafael, California: Morgan & Claypool Publishers.

[20] Zuo, J. M., & Spence, J. C. (20017) *Advanced transmission electron microscopy imaging and diffraction in nanoscience*. New York, New York: Springer.

[21] Theocaris, P. S. (1969). *Moiré fringes in strain analysis.* Oxford: Pergamon Press.

[22] Budynas, R. G., Nisbett, J. K., & Shigley, J. E. (2011) *Shigley's mechanical engineering design*. New York: McGraw-Hill.

[23] Deepak, F. L., Mayoral, A., & Arenal, R. (Eds.). (2005). *Advanced transmission electron microscopy: Applications to nanomaterials.* Switzerland: Springer.

APPENDIX A: EXPERIMENTAL DATA

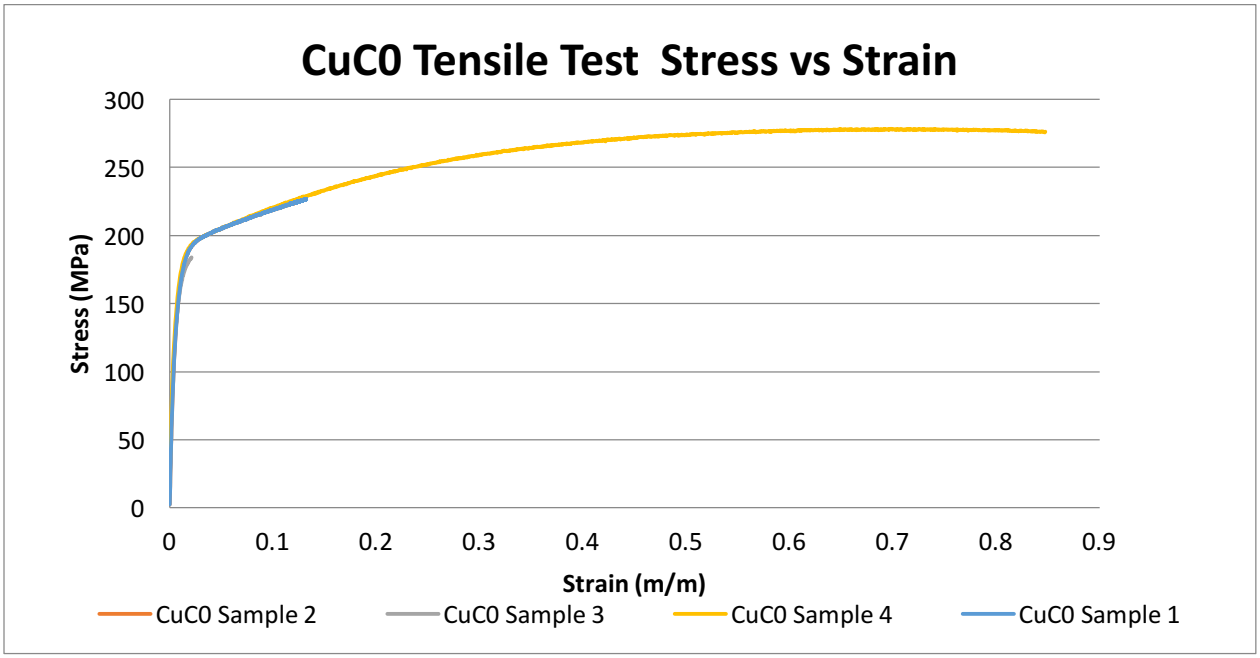

Figure A.1 Tensile test stress versus strain graph for copper sample with 0 percent added carbon.

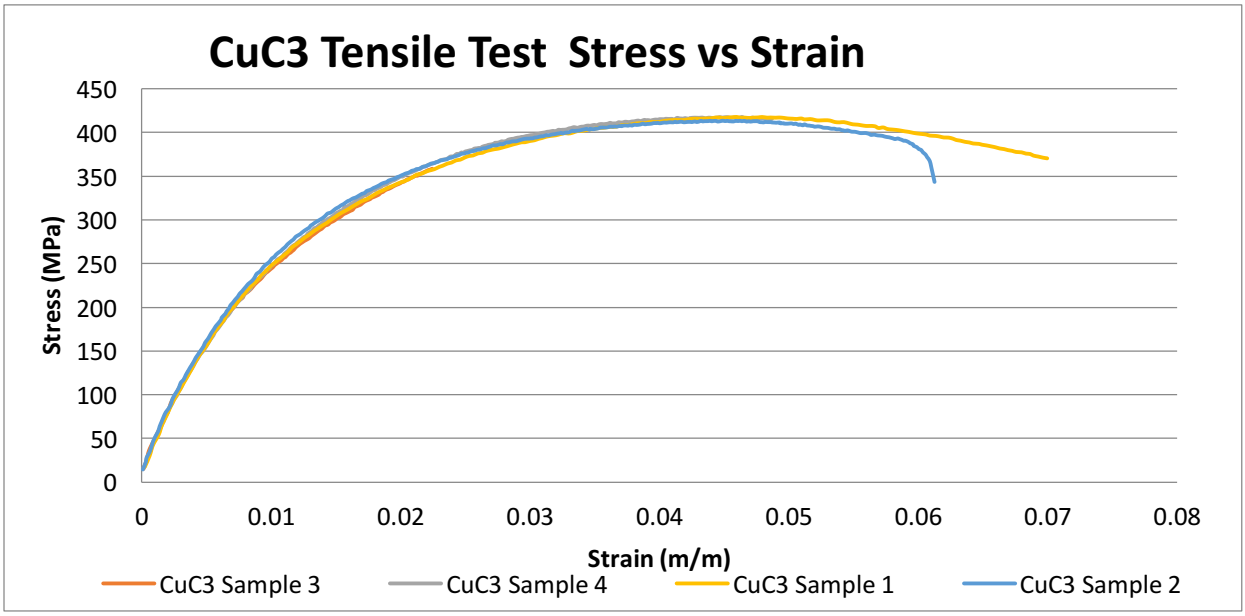

Figure A.2 Tensile test stress versus strain graph for copper sample with 3 percent added carbon.

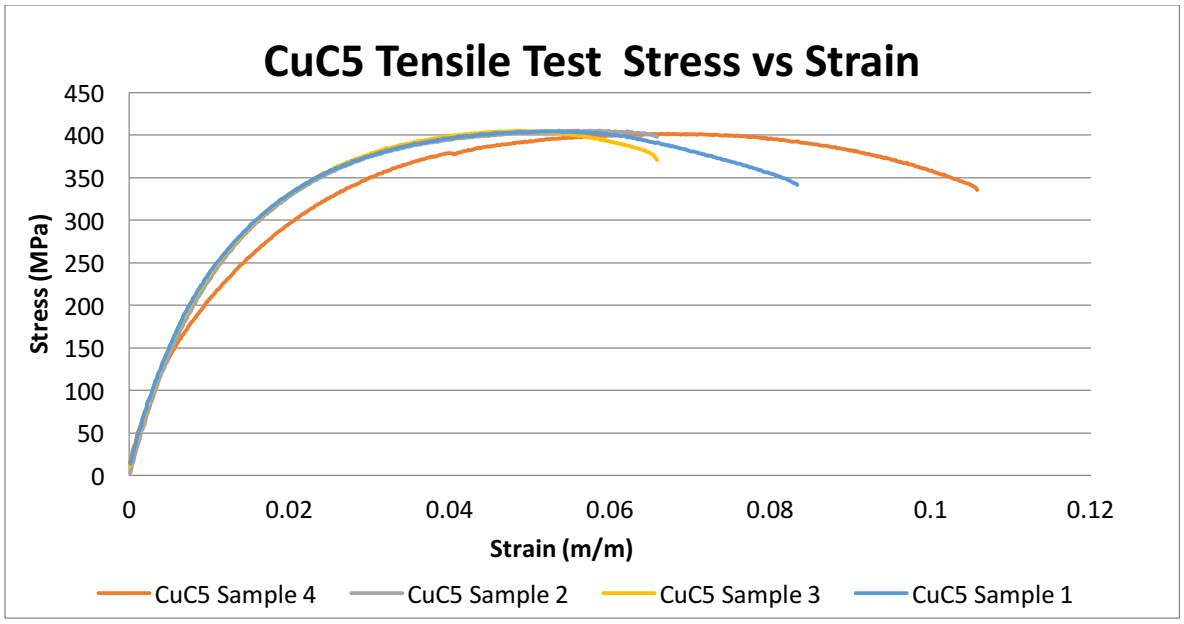

Figure A.3 Tensile test stress versus strain graph for copper sample with 5 percent added carbon.

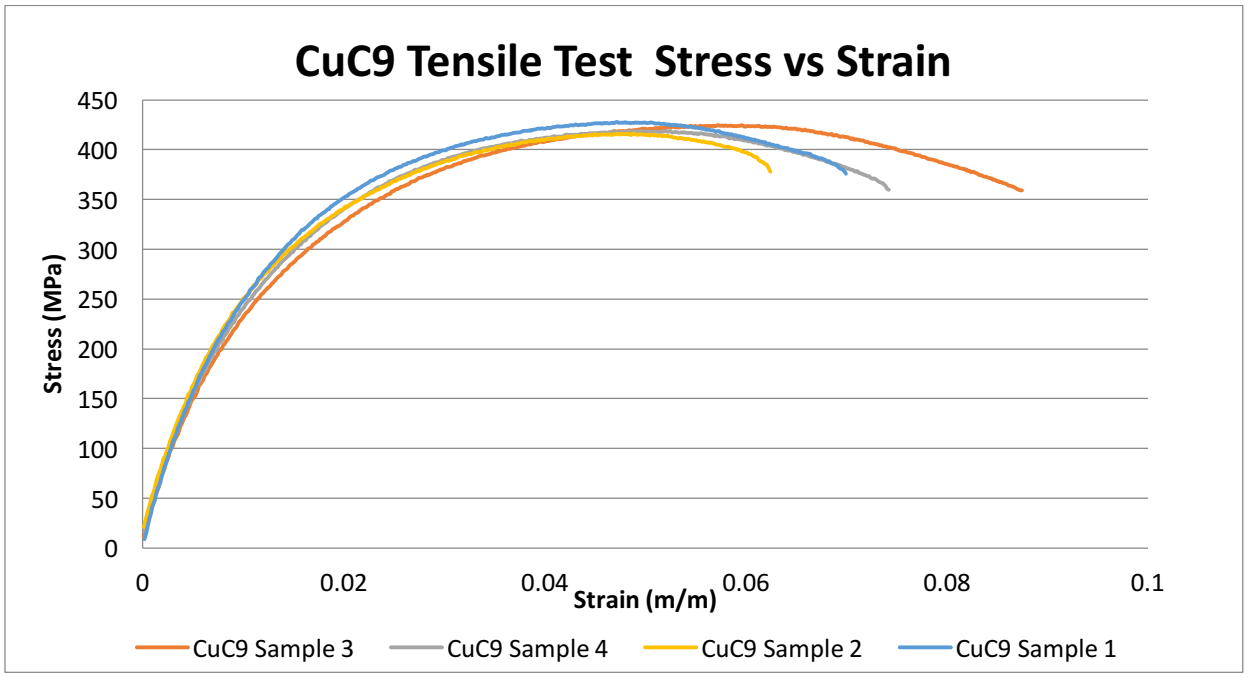

Figure A.4 Tensile test stress versus strain graph for copper sample with 9 percent added carbon.

Table A.1 Results from tensile test performed on copper wires.

Added weight percent of carbon	Specimen	Max Load (N)	Max Total Displacement (cm)	UTS (MPa)	Elongation of Specimen (cm)	Strain at Fracture	Yield Stress (MPa)	Elastic Modulus (MPa)
0	Sample 1	2050.63	2.28	276.56	2.27	0.17	0.10	34.87
	Sample 2	2050.63	2.45	272.04	2.44	0.18	0.13	34.42
	Sample 3	2068.42	2.26	278.95	2.26	0.17	0.14	31.21
	Sample 4	2068.42	2.36	278.95	2.36	0.18	0.12	29.18
3	Sample 1	3211.62	0.19	419.16	0.14	0.01	0.21	35.54
	Sample 2	3180.48	0.16	415.09	0.14	0.01	0.22	36.78
	Sample 3	3224.96	0.19	420.90	0.13	0.01	0.22	34.08
	Sample 4	3211.62	0.19	419.16	0.14	0.01	0.22	33.74
5	Sample 1	3167.13	0.22	406.71	0.19	0.01	0.21	33.85
	Sample 2	3171.58	0.17	407.28	0.13	0.01	0.20	32.46
	Sample 3	3167.13	0.17	406.71	0.13	0.01	0.21	32.71
	Sample 4	3140.44	0.27	403.28	0.17	0.01	0.18	31.31
9	Sample 1	3345.06	0.19	429.56	0.14	0.01	0.21	36.13
	Sample 2	3309.48	0.18	418.21	0.13	0.01	0.22	34.69
	Sample 3	3318.37	0.24	426.13	0.18	0.01	0.19	34.41
	Sample 4	3327.27	0.21	420.46	0.15	0.01	0.22	33.88

Table A.2 Results and measurements from nanoindentation test performed on copper with 0 percent added carbon at a maximum load of 10,000 uN.

Indent	A_{total} (nm^2)	A_{OP} (nm^2)	A_{PU} (nm^2)	$b_{average}$ (nm)	b_1 (nm)	b_2 (nm)	b_3 (nm)	a_1 (nm)	a_2 (nm)	a_3 (nm)	S (μN/nm)	P_{max} (μN)
1	6130634	6827092.05	696458.5	3830.60	3994.59	3953.65	3543.55	160.5	90.7	-19.7	340.19	10000.48
2	5757775	6573243.90	815469	3700.34	3849.74	3713.03	3538.27	138.8	91.6	50.2	339.40	10000.44
3	6103601	6652818.97	549217.7	3612.11	3808.16	3724.84	3303.34	62.4	72.1	59.1	350.39	10000.20
4	6089956	6737791.20	647834.9	3818.85	3988.43	3936.72	3531.41	80.5	75.9	59.6	351.36	10000.42
5	5243571	6482895.90	1239324	3727.86	3860.73	3812.21	3510.62	89.5	247.4	86.4	373.50	10000.02
6	6170383	6805599.95	635216.5	3751.42	3885.67	3844.69	3523.89	72.2	71.4	72.0	344.10	10000.48
7	5003548	5829882.67	826335.1	3496.68	3625.27	3657.23	3207.55	155.7	93.7	51.5	332.09	10000.27
8	5646910	6782057.99	1135148	3806.57	3936.42	3998.46	3484.85	81.8	245.1	52.8	344.43	10000.23
9	5294058	6620300.07	1326242	3760.12	3925.77	3946.13	3408.47	91.8	302.6	54.7	354.26	10000.28

Table A.3 Corrected and uncorrected values of elastic modulus and hardness from nanoindentation test performed on copper with 0 percent added carbon at a maximum load of 10,000 uN.

Indent	Hardness uncorrected (GPa)	Hardness corrected (GPa)	E uncorrected (GPa)	E corrected (GPa)	E_r uncorrected (GPa)	E_r corrected (GPa)
1	1.46	1.63	116.73	123.98	115.35	121.76
2	1.52	1.73	118.90	128.08	117.29	125.35
3	1.50	1.63	122.38	128.47	120.36	125.69
4	1.48	1.64	121.90	129.03	119.93	126.18
5	1.54	1.90	133.40	150.53	129.97	144.54
6	1.46	1.62	118.43	125.12	116.86	122.76
7	1.71	1.99	124.09	135.26	121.85	131.56
8	1.47	1.77	118.78	131.65	117.18	128.45
9	1.51	1.88	124.24	140.95	121.98	136.44

Table A.4 Results and measurements from nanoindentation test performed on copper with 3 percent added carbon at a maximum load of 10,000 uN.

Indent	A_{total} (nm^2)	A_{OP} (nm^2)	A_{PU} (nm^2)	$b_{average}$ (nm)	b_1 (nm)	b_2 (nm)	b_3 (nm)	a_1 (nm)	a_2 (nm)	a_3 (nm)	S (μN/nm)	P_{max} (μN)
1	6092191	6188735.64	96545.14	3482.4	3543.586	3550.69	3352.92	12.6	3.8	18.9	183.01	9999.95
2	5727868	5903199.87	175332	3300.50	3389.41	3383.78	3128.32	36.94	25.9	4.8	182.64	10000.17
3	6635069	7180185.89	545117	3774.45	3855.606	3832.20	3635.56	55.52	79.38	48.99	198.42	10000.4
4	5670501	6184771.31	514270.3	3463.86	3509.672	3561.40	3320.51	77.03	71.57	40.44	197.36	10000.37
5	6615017	6927172.62	312156.1	3860.72	3912.125	3900.46	3769.57	37.31	21.91	43.73	189.09	10000.27
6	5656057	5815166.46	159109	3394.60	3428.411	3492.80	3262.59	10.03	8.33	41.32	186.86	10000.12
7	6465346	6981479.16	516133.1	3835.98	3884.907	3862.18	3760.85	56.45	58.96	55.91	205.18	10000.27
8	5137456	5296623.25	159167.1	3105.00	3179.072	3101.61	3034.33	19.36	26.88	19.03	183.04	9999.85
9	5992871	6602606.01	609735	3823.31	3722.848	3812.57	3934.51	71.16	66.5	65.4	197.37	10000.5

Table A.5 Corrected and uncorrected values of elastic modulus and hardness from nanoindentation test performed on copper with 3 percent added carbon at a maximum load of 10,000 uN.

Indent	Hardness uncorrected (GPa)	Hardness corrected (GPa)	E uncorrected (GPa)	E corrected (GPa)	E_r uncorrected (GPa)	E_r corrected (GPa)
1	1.61	1.64	62.89	63.43	65.18	65.71
2	1.69	1.74	64.34	65.40	66.60	67.63
3	1.39	1.50	63.33	66.06	65.61	68.26
4	1.61	1.76	68.16	71.41	70.31	73.44
5	1.44	1.51	61.33	62.86	63.65	65.15
6	1.71	1.76	66.46	67.46	68.65	69.63
7	1.43	1.54	66.61	69.41	68.80	71.51
8	1.88	1.94	68.32	69.46	70.46	71.56
9	1.51	1.66	65.84	69.34	68.05	71.45

Table A.6 Results and measurements from nanoindentation test performed on copper with 5 percent added carbon at a maximum load of 10,000 uN.

Indent	A_{total} (nm^2)	A_{OP} (nm^2)	A_{PU} (nm^2)	$b_{average}$ (nm)	b_1 (nm)	b_2 (nm)	b_3 (nm)	a_1 (nm)	a_2 (nm)	a_3 (nm)	S (μN/nm)	P_{max} (μN)
1	3727160	3987988.52	260828.7	2769.86	2850.43	2720.90	2738.26	62.5	67.8	-10.4	231.61	9999.92
2	4882552	4973073.31	90521	3123.53	3193.9	3040.80	3135.88	37.5	13.3	-13.9	248.02	10000.59
3	6017757	6203608.99	185851.8	3629.46	3756.00	3562.37	3570	51.4	11.6	2.2	284.55	9999.89
4	4883590	4991781.37	108191.4	3196.23	3224.90	3130.06	3233.72	28.4	18	-3.3	251.90	10000.24
5	4495210	4603930.91	108721.2	2955.42	2972.15	2910	2984.12	20.85	11.96	14.03	359.23	10000.35
6	4727555	4865994.76	138440.3	3065.61	3123.28	3041.33	3032.22	15.7	9	32.8	308.04	10000.11
7	4253839	4374945.86	121106.4	2983.78	3034.02	2960.27	2957.05	2.99	17.79	30.9	189.15	10000.45
8	5494376	5757187.37	262811.6	3418.10	3585.03	3343.83	3325.43	12.2	38.9	46.8	333.23	9999.90
9	5686000	5859367.61	173367.6	3417.10	3517.74	3351.20	3382.36	50.8	3.9	9.9	299.66	10000.03

Table A.7 Corrected and uncorrected values of elastic modulus and hardness from nanoindentation test performed on copper with 5 percent added carbon at a maximum load of 10,000 uN.

Indent	Hardness uncorrected (GPa)	Hardness corrected (GPa)	E uncorrected (GPa)	E corrected (GPa)	E_r uncorrected (GPa)	E_r corrected (GPa)
1	2.50	2.68	102.72	106.64	102.76	106.32
2	2.01	2.04	98.10	99.12	98.53	99.47
3	1.61	1.66	101.04	102.76	101.22	102.79
4	2.00	2.04	99.59	100.81	99.89	101.02
5	2.17	2.22	155.06	157.25	148.33	150.15
6	2.05	2.11	126.22	128.31	123.72	125.55
7	2.28	2.35	78.39	79.61	80.12	81.27
8	1.73	1.82	125.45	128.81	123.05	125.98
9	1.70	1.75	110.38	112.26	109.68	111.37

Table A.8 Results and measurements from nanoindentation test performed on copper with 9 percent added carbon at a maximum load of 10,000 uN.

Indent	A_{total} (nm^2)	A_{OP} (nm^2)	A_{PU} (nm^2)	$b_{average}$ (nm)	b_1 (nm)	b_2 (nm)	b_3 (nm)	a_1 (nm)	a_2 (nm)	a_3 (nm)	S (μN/nm)	P_{max} (μN)
1	6962755	7608762.97	646008.4	3506.17	3582.86	3450.92	3484.72	77.9	83.7	73	170.64	9999.86
2	6785012	7417711.43	632699.6	3470.92	3523.89	3350.06	3538.82	91.8	67.7	72.6	164.39	9999.81
3	5673252	6334304.83	661052.7	3600.09	3763.00	3410.36	3626.92	69.8	92.1	71.9	152.72	10000.06
4	6650003	7183274.44	533271.8	3532.79	3788.85	3260.75	3548.77	65.9	59.9	66.4	179.26	9999.83
5	6685353	7190726.77	505374.3	3346.23	3463.01	3332.16	3243.53	78.8	84.9	28.6	169.77	10000.71
6	6557587	7098283.80	540696.4	3623.45	3810.77	3423.74	3635.84	53	70.4	66.6	177.54	10000.65
7	6281045	6875767.03	594722.4	3456.16	3671.51	3275.51	3421.47	78.9	57.8	82.4	161.56	10000
8	6593328	7257282.09	663954.5	3500.61	3665.31	3351.80	3484.72	79	65	97.5	154.05	9999.93
9	5780675	6460716.82	680041.8	3616.88	3728.64	3480.23	3641.77	99.7	176.1	-36.4	154.48	10000.15

Table A.9 Corrected and uncorrected values of elastic modulus and hardness from nanoindentation test performed on copper with 9 percent added carbon at a maximum load of 10,000 uN.

Indent	Hardness uncorrected (GPa)	Hardness corrected (GPa)	E uncorrected (GPa)	E corrected (GPa)	E_r uncorrected (GPa)	E_r corrected (GPa)
1	1.31	1.43	52.38	54.89	54.81	57.31
2	1.34	1.47	51.04	53.50	53.47	55.93
3	1.57	1.76	51.33	54.40	53.76	56.82
4	1.39	1.50	56.87	59.24	59.26	61.60
5	1.39	1.49	53.67	55.78	56.09	58.18
6	1.40	1.52	56.64	59.08	59.04	61.44
7	1.45	1.59	52.16	54.71	54.59	57.13
8	1.37	1.51	48.24	50.73	50.66	53.16
9	1.54	1.72	51.41	54.52	53.84	56.94

Table A.10 Results and measurements from nanoindentation test performed on copper with 0 percent added carbon at a maximum load of 5,000 uN.

Indent	A_{total} (nm^2)	A_{OP} (nm^2)	A_{PU} (nm^2)	$b_{average}$ (nm)	b_1 (nm)	b_2 (nm)	b_3 (nm)	a_1 (nm)	a_2 (nm)	a_3 (nm)	S (μN/nm)	P_{max} (μN)
1	2727906	2968543.15	240637.3	2163.82	2228.00	2301.84	1961.63	29.7	34.1	77.8	220.99	4998.82
2	2496833	2768527.46	271694.3	2404.04	2494.47	2191.46	2526.20	48.4	57.2	38.3	193.76	4999.03
3	1897237	2222942.33	325705.3	2186.15	2110.92	2227.03	2220.49	51.9	62.7	75.1	186.52	4999.07
4	2562539	2852422.09	289883.5	1959.14	1917.08	1958.29	2002.04	71.7	44.1	72.6	245.11	4998.92
5	2143398	2426242.88	282844.7	2138.59	2163.35	2028.00	2224.43	68.9	44.5	55	215.93	4999.11
6	2301902	2597855.29	295953.5	2353.72	2454.58	2224.45	2382.12	45.1	66.7	48.3	210.78	4998.79
7	2026242	2154047.28	127805	1838.77	1894.75	1842.96	1778.59	9.7	54	24.8	226.76	4998.82
8	2820876	2989284.99	168409.2	2210.63	2152.44	2199.11	2280.35	25.9	22	49.1	267.83	4998.99
9	2423922	2630998.35	207076.2	2021.97	2083.55	1932.56	2049.80	44.6	66.8	19	261.43	4998.99

Table A.11 Corrected and uncorrected values of elastic modulus and hardness from nanoindentation test performed on copper with 0 percent added carbon at a maximum load of 5,000 uN.

Indent	Hardness uncorrected (GPa)	Hardness corrected (GPa)	E uncorrected (GPa)	E corrected (GPa)	E_r uncorrected (GPa)	E_r corrected (GPa)
1	1.683933	1.832478	114.8031	120.3639	113.642736	118.5775257
2	1.805667	2.002152	103.1834	109.2542	103.176339	108.6709541
3	2.248857	2.634926	111.6708	121.9862	110.842024	120.008349
4	1.752519	1.95077	131.8073	140.0754	128.585743	135.6963648
5	2.060433	2.33233	125.1967	134.2682	122.828146	130.712558
6	1.924202	2.171595	117.3042	125.531	115.868136	123.1209067
7	2.320668	2.467044	141.4821	146.5331	136.896183	141.1812343
8	1.672304	1.772142	141.8989	146.7004	137.251176	141.3225492
9	1.900036	2.062356	148.4544	155.6355	142.8016	148.8119265

Table A.12 Results and measurements from nanoindentation test performed on copper with 3 percent added carbon at a maximum load of 5,000 uN.

Indent	A_{total} (nm^2)	A_{OP} (nm^2)	A_{PU} (nm^2)	$b_{average}$ (nm)	b_1 (nm)	b_2 (nm)	b_3 (nm)	a_1 (nm)	a_2 (nm)	a_3 (nm)	S (μN/nm)	P_{max} (μN)
1	1924963	2063605.38	138642.6	1563.6	1623.08	1547.19	1520.52	43.6	50.5	18.8	160.52	4998.96
2	3005840	3178573.23	172733.3	2116.81	2116.97	2036.29	2197.18	35.8	55.1	13	205.61	4998.97
3	2501672	2570342.65	68670.9	1617.40	1610.03	1593.8	1648.39	19.1	37.1	-2.14	178.59	4998.81
4	2900426	3004920.17	104493.9	2111.56	2118.79	2040.83	2175.06	12.98	32.32	17.71	195.46	4998.99
5	2684699	2736447.84	51748.5	1728.49	1673.70	1705.75	1806.01	5.32	30.1	2.7	187.75	4998.97
6	2551523	2586549.60	35026.31	1636.63	1611.86	1593.8	1704.23	7.11	22.13	-1.99	169.95	4999.06
7	2779196	2817301.59	38105.8	1752.86	1732.19	1780.16	1746.22	1.94	18.3	7.44	180.71	4998.90
8	2855576	2974907.52	119331.5	1955.24	1925.09	2005.64	1934.99	26.01	20.51	31.19	174.43	4998.89
9	2888656	2951270.69	62615.02	1971.95	2024.74	1905.17	1985.95	25.73	12.38	2.32	188.52	4998.76

Table A.13 Corrected and uncorrected values of elastic modulus and hardness from nanoindentation test performed on copper with 3 percent added carbon at a maximum load of 5,000 uN.

Indent	Hardness uncorrected (GPa)	Hardness corrected (GPa)	E uncorrected (GPa)	E corrected (GPa)	E_r uncorrected (GPa)	E_r corrected (GPa)
1	2.42	2.59	98.61	102.47	99.00	102.53
2	1.57	1.66	102.09	105.30	102.18	105.10
3	1.94	1.99	98.28	99.77	98.69	100.06
4	1.66	1.72	99.59	101.57	99.90	101.71
5	1.82	1.86	100.31	101.39	100.55	101.54
6	1.93	1.95	92.78	93.50	93.62	94.29
7	1.77	1.79	94.69	95.42	95.39	96.06
8	1.68	1.75	88.45	90.46	89.60	91.47
9	1.69	1.73	96.68	97.84	97.22	98.29

Table A.14 Results and measurements from nanoindentation test performed on copper with 5 percent added carbon at a maximum load of 5,000 uN.

Indent	A_{total} (nm^2)	A_{OP} (nm^2)	A_{PU} (nm^2)	$b_{average}$ (nm)	b_1 (nm)	b_2 (nm)	b_3 (nm)	a_1 (nm)	a_2 (nm)	a_3 (nm)	S (μN/nm)	P_{max} (μN)
1	2738606	2987391.44	248785.1	2114.63	2264.155	2042.96	2036.78	31.7	68.6	49.5	261.44	4998.71
2	3048977	3271087.92	222111.4	2225.09	2354.761	2276.35	2044.16	14.9	73.4	38.8	249.78	4999.07
3	3107269	3376209.03	268940.4	2258.81	2504.496	2221.93	2050	58.4	46.6	46.6	251.52	4999.15
4	2900074	3088213.85	188139.9	2243.01	2479.879	2115.32	2133.84	21.9	34.6	50.3	249.01	4998.78
5	2797764	3010703.29	212938.9	2278.40	2516.446	2219.03	2099.73	41.1	39	38.9	249.46	4998.65
6	2575322	2840486.37	265164.3	2234.46	2446.242	2153.34	2103.80	47	45.8	58.3	254.74	4998.83
7	2767523	3010130.51	242607.4	2195.49	2414.477	2239.86	1932.14	36.9	54	49.8	249.36	4998.91
8	2602719	2857357.66	254638.2	2278.46	2595.997	2250.08	1989.29	58.1	37.1	47.1	241.69	4999.23
9	2860426	3024497.14	164071.5	2136.07	2387.3	2040.83	1980.10	25.9	39.4	32.5	244.60	4999.25

Table A.15 Corrected and uncorrected values of elastic modulus and hardness from nanoindentation test performed on copper with 5 percent added carbon at a maximum load of 5,000 uN.

Indent	Hardness uncorrected (GPa)	Hardness corrected (GPa)	E uncorrected (GPa)	E corrected (GPa)	E_r uncorrected (GPa)	E_r corrected (GPa)
1	1.67	1.82	138.11	145.14	134.02	140.00
2	1.52	1.63	124.66	129.71	122.36	126.77
3	1.48	1.60	123.43	129.35	121.28	126.45
4	1.61	1.72	128.31	132.96	125.54	129.58
5	1.66	1.78	130.41	135.96	127.38	132.17
6	1.75	1.94	137.99	145.93	133.91	140.67
7	1.66	1.80	130.37	136.73	127.34	132.83
8	1.74	1.92	129.61	136.65	126.68	132.76
9	1.65	1.74	127.24	131.32	124.61	128.17

Table A.16 Results and measurements from nanoindentation test performed on copper with 9 percent added carbon at a maximum load of 5,000 uN.

Indent	A_{total} (nm^2)	A_{OP} (nm^2)	A_{PU} (nm^2)	$b_{average}$ (nm)	b_1 (nm)	b_2 (nm)	b_3 (nm)	a_1 (nm)	a_2 (nm)	a_3 (nm)	S (μN/nm)	P_{max} (μN)
1	3900195	4030930.01	130734.7	1672.98	1552.93	1645.84	1820.16	28.1	39.7	31.7	134.41	4998.65
2	3645020	3931242.21	286222.4	1954.10	2109.50	1874.51	1878.29	28.2	87.7	70.6	117.44	4999.08
3	3216569	3332598.06	116029.6	1711.90	1870	1588.08	1677.64	4.6	56.5	25.2	101.88	4999.61
4	3734450	3941741.96	207291.7	1824.04	1877.71	1810.02	1784.40	59.7	63.4	21.6	120.47	4999.48
5	3117725	3326472.91	208747.7	1717.01	1856.07	1611.52	1683.44	48.4	74.3	32.1	139.38	4998.96
6	3551797	3754238.74	202442	2173.57	2308.46	2112.06	2100.21	26.65	61.32	30.62	119.52	4999.28
7	3371108	3612728.38	241620	2092.85	2244.14	2075.42	1958.97	21.1	67.4	58.5	135.07	4999.08
8	3177934	3387948.68	210014.9	1967.53	2074.72	1962.54	1865.31	28.24	78.79	28.88	135.23	4998.59
9	3149728	3407847.12	258119.2	2094.69	2180	2100.38	2003.69	47.75	57.2	51.95	126.49	4998.7

Table A.17 Corrected and uncorrected values of elastic modulus and hardness from nanoindentation test performed on copper with 9 percent added carbon at a maximum load of 5,000 uN.

Indent	Hardness uncorrected (GPa)	Hardness corrected (GPa)	E uncorrected (GPa)	E corrected (GPa)	E_r uncorrected (GPa)	E_r corrected (GPa)
1	1.24	1.28	56.92	57.93	59.31	60.31
2	1.27	1.37	50.04	52.08	52.47	54.51
3	1.50	1.55	47.02	47.92	49.44	50.34
4	1.26	1.33	51.33	52.82	53.76	55.24
5	1.50	1.60	65.48	67.80	67.71	69.95
6	1.33	1.40	52.23	53.78	54.65	56.20
7	1.38	1.48	60.63	62.91	62.96	65.19
8	1.47	1.57	62.80	64.99	65.09	67.22
9	1.46	1.58	58.33	60.83	60.70	63.16

Table A.18 Microindentor result measurement for copper samples with varying added weight percent of carbon.

Sample	d_1	d_2	HV_{500}
CuC0	90.6	88.55	115.57
	91.2	88.25	115.20
	93.5	92.5	107.20
	92.5	92.25	108.65
	89	89	117.05
	89	90	115.75
	89	90.5	115.11
	89.5	89.75	115.42
CuC3	89.75	86	120.12
	88	85.5	123.23
	87.5	87.25	121.45
	90.5	87.75	116.75
	90.75	89.5	114.15
	86.5	89.5	119.76
	90.75	92	111.05
	89.5	88.5	117.05
CuC5	92.5	90	111.37
	92	88.75	113.55
	89.25	88.75	117.05
	91.5	86.75	116.81
	90	87.28	118.03
	93	92.25	108.07
	91.5	93.25	108.66
	90.5	90	113.83
CuC9	87	88	121.10
	92.5	88.25	113.58
	86.5	90.25	118.77
	89.25	86.5	120.10
	88.5	90.25	116.08
	90.5	88.75	115.44
	87.5	90.75	116.76
	91.0	88.25	115.45